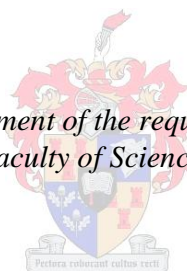


**THEORETICAL INVESTIGATION OF
DIELECTROPHORESIS AND
ELECTROPHORESIS
AS TECHNIQUES FOR SILVER
DEFLECTIONS**

by

Naphtali Malesela Mokgalapa

*Thesis presented in fulfilment of the requirements for the degree of
Master of Science in the Faculty of Science at Stellenbosch University*



Supervisors:
Prof. Shaun M. Wyngaardt
Mr. Robert Thomas Dobson

December 2012

Declaration

By submitting this thesis/dissertation electronically, I declare that the entirety of the work contained therein is my own, original work, that I am the sole author thereof (save to the extent explicitly otherwise stated), that reproduction and publication thereof by Stellenbosch University will not infringe any third party rights and that I have not previously in its entirety or in part submitted it for obtaining any qualification.

December 2012

Copyright © 2012 Stellenbosch University

All rights reserved

Acknowledgements

During the time that I have spent on this project, there are many people who have helped me, in one way or another. In particular, I wish to thank Professor Shaun Wyngaardt, my principal research advisor, for many of his suggestions on this research, for his guidance during the course of this work and for allowing me the maximum freedom in researching on this topic. Also, my gratitude goes to my co-advisor Mr. Robert Dobson for the insightful discussions that we had throughout the course of this research.

I would like to thank the Department of Physics for its support of this research and for having made such a lively working and social environment for me. My sincere thanks are given to the staff of the Physics department and to all the graduate students in the department who provided me with assistance during this work. Special thanks to Dr. Toafiq Ibrahim and Mr. Hermanus Steyn for contributions on programming and Nolubabalo Khula for her help with drawings. Most of all I am greatly indebted to the love of my life, Nomahlubi Manakaza for her constant love and support over the years I was studying and for putting up with me when I have been at my most insufferable. To my parents, thank you for your prayers and support. I am thankful for the grant support from the following organizations, the department of physics Stellenbosch university, department of Mechanical engineering through Mr. Dobson, National Research Fund and Nuclear Institute of Theoretical Physics. Finally, I would like to thank the department of Electrical Engineering at the University of Stellenbosch especially Professor J. P. Holtzhausen who assisted in this thesis making available a software called Electro V6.7 used for dielectrophoresis calculations.

Once the realization is accepted that even between the closest human beings infinite distances continue to exist, a wonderful living side by side can grow up, if they succeed in loving the distance between them which makes it possible for each to see the other whole against the sky. *Rilke*

This work is dedicated to my family, my mother, Mary Mokhalapa, my little brothers, Baleseng and Gontse Mokgalapa, my sister, Aniki Mokhalapa and my Knees' Bontle and Amogelang, Nomahlubi and my daughter Lesedi. Most of all I would like to say thank you to my grandparents Naphtali and Elizabeth Mokgalapa who have been instrumental in my upbringing, and taught me to always value education and respect others. Without your constant reminders and love I would'nt have made it this far, may your souls rest in peace and thank you.

Abstract

The primary circuit components of very high temperature reactors (VHTRs) experience various unwanted fission products such as Kr, Xe, I, Cs, Sr, and Ag. These particles are generated during normal operation of the reactor from ablation, cracks and/or defects are transported by the helium coolant. The main candidate that has been identified as a cause for concern and the focus of research to minimizing radioactive contamination of the reactor coolant circuit is silver. This is because the design of the coated particles limits the release of fission products into the coolant except for silver (Ag^{110m}). Ag^{110m} is a long lived metallic fission product formed inside the nuclear reactor core and is the only known element released out of the coated particles into the coolant at any temperature above 1150 °C when the reactor starts to heat up. The release occurs on intact coated particles, failed particles and also from defective particles. The amount of released silver is initially small and occurs as the pebble heats up and this is strongly dependent on the temperature of the core. It is therefore able to reach the surface of the reactor core and enter into the Helium coolant flowing throughout the reactor. Thus Ag^{110m} will be circulated through the reactor circuit until it reaches the cooler sides of the main power system (MPS) where it will start to plate out. The presence of this radioactive silver in the primary circuit components may result in unwanted maintenance problems from a radiation hazard point of view. The development of a method to remove particles from the helium stream is therefore needed.

In this work, two theoretical deflection models used to deflect the silver particles are proposed, namely the stochastic and the deterministic deflection models. The latter describes the deflection of microparticles in a helium medium. It uses the dielectrophoresis (DEP) technique to investigate the deflection of a silver

particle with a radius of $3 \mu\text{m}$. It is observed from this model that a silver microparticle with a radius of $3 \mu\text{m}$ moving in a helium medium with the bulk velocity of 0.021 ms^{-1} and subjected to a dielectrophoretic force only deflect an amount of 0.52039 nm and 4.49882 nm in the x - and z -directions on average.

The former (stochastic deflection model) describes the deflection of ions and polarized particles by using probability theory, namely kinetic theory of gases. This model showed that the mean free time that the particle spends while deflected by a uniform electric field is short so much that there is not enough time for a silver particle to be appreciably deflected between collisions. For example, when an electric field of 100kV/m was applied on a single silver ion for a time of $0.1 \mu\text{s}$, the deflection distance obtained was 33.38 nm for a free time of 0.189285 ns and under pressure and temperature conditions of 1 bar and 20° C .

The Brownian motion was then compared to the effects of a nonuniform electric field in polarizing and deflecting an atom. This is done by comparing the Brownian motion and the polarizability of an atom using nonuniform electric fields. It is found that the silver speed produced from Brownian motion (79.563 ms^{-1}) is far larger than that produced from the polarizability of an atom ($4.69455 \times 10^6 \text{ nms}^{-1}$). The deterministic and stochastic deflection models using nonuniform electric fields proved that the dielectrophoresis technique is negligibly small in deflecting particles and cannot be used to deflect silver particles as required in a VHTR.

Opsomming

Die primêre siklus komponente van baie ho temperatuur reaktore (VHTRs) word blootgestel aan verskeie ongewenste fisie produkte soos Kr, Xe, I, Cs, Sr, en Ag. Hierdie deeltjies word gegeneer gedurende normale werking van die reaktor van abarasie, krake en / of defekte word vervoer deur die helium verkoelingsmiddel. Die belangrikste kandidaat wat gidentifiseer is as 'n rede vir kommer en die fokus van navorsing op die minimalisering van radioaktiewe besoedeling van die reaktor verkoelingsmiddel siklus is silwer. Die rede hiervoor is die ontwerp van die omhulsel wat die vrylating van die fisie produkte in die koelmiddel behalwe vir silwer (Ag^{110m}) beperk. Ag^{110m} is 'n metaal fisie-produk met 'n lang leeftyd wat gevorm word binne-in die kern van die reaktor en is sover bekend die enigste element wat vrygestel word deur die bedekte deeltjies in die verkoelingsmiddel by enige temperatuur bo $1150\text{ }^{\circ}\text{C}$ wanneer die reaktor begin verhit. Die vrystelling kom voor by ongeskonde brandstofomhulse, nie funksionele deeltjies en ook van gebrekkige deeltjies. Die bedrag van vrygestel silwer is aanvanklik klein en kom voor as die brandstofelemente verhit en heirdie vrystelling is sterk afhanklik van die temperatuur van die kern. Dit is dus in staat om die oppervlak van die reaktor kern te bereik en betree die Helium verkoelingsmiddel vloeistelsel en beweeg regdeur die reaktor. Dus sirkuleer die Ag^{110m} deur die reaktor kring totdat dit die koeler kante van die MPS bereik waar dit sal begin uitplaat. Die teenwoordigheid van hierdie radioaktiewe silwer in die primêre stroombaan komponente kan lei tot ongewenste onderhoud probleme van 'n straling gevaar oopspoor. Die ontwikkeling van 'n metode om deeltjies te verwyder uit die helium stroom is dus nodig.

In hierdie werk word van twee teoretiese defleksie modelle gebruik gemaak om die silwer partikels se defleksie te beskryf, naamlik die stogastiese en die deterministiese defleksie modelle. Laasgenoemde beskryf die

defleksie van mikro grootte partikel in 'n helium medium. Dit maak gebruik van die dielektroflorosensie (DEP) tegniek om ondersoek in te stel na die defleksie van 'n silwer deeltjie met 'n radius van $3 \mu\text{m}$. Dit is vanaf hierdie model waargeneem dat 'n silwer mikrodeeltjie met 'n radius van 3 m in 'n helium medium beweeg met die snelheid van $0,021 \text{ ms}^{-1}$ en onderworpe is aan 'n dielektroforetiese krag dit net met 'n gemiddelde van $0,52039 \text{ nm}$ en $4,49882 \text{ nm}$ in die x - en z -rigtings deflekteer. Die voormalige (stogastiese defleksie model) beskryf die defleksie van ione en gepolariseerde partikels deur gebruik te maak van waarskynlikheidsteorie, naamlik die kinetiese teorie van gasse. Hierdie model toon dat die gemiddelde vrye tyd wat die deeltjie spandeer terwyl dit gedeflekteer word deur 'n uniforme elektriese veld sovel korter is dat daar nie genoeg tyd is vir 'n silwer deeltjie is om aansienlik tussen botsings gedeflekteer kan word nie. Byvoorbeeld, wanneer 'n elektriese veld van 100kV/m toegepas word op 'n enkele silwer ioon vir 'n tyd van $0.1 \mu\text{s}$, die defleksie afstand van $33,38 \text{ mm}$ verkry word vir 'n vrye tyd van 0.189285 ns en onder druk en temperatuur voorwaardes van 1 bar en $20 \text{ }^\circ\text{C}$. Die Brown-beweging was dan vergeleke met die uitkoms van 'n uniforme elektriese veld wat 'n polariserende atoom deflekteer. Dit word gedoen deur die vergelykings van die Brown-beweging en die polariseerbaarheid van 'n atoom met behulp van nie-uniforme elektriese veld te gebruik. Daar word gevind dat as die silwer spoed van Brown se beweging ($79,563 \text{ ms}^{-1}$) veel groter is as di van die polariseerbare atoom ($4,69455 \times 10^{-6} \text{ nms}^{-1}$). Die deterministiese en stogastiese defleksie modelle deur gebruik te maak van nonuniforme elektriese velde bewys dat dielectrophoresis tegniek is weglaatbaar klein in defleksie van deeltjies en kan dus nie gebruik word om silwer partikels te buig soos wat in 'n VHTR vereis word nie.

Contents

Acknowledgements	i
Abstract	iv
Opsomming	vi
List of figures	xi
List of tables	xiv
1 Introduction	1
1.1 Background	1
1.1.1 Very High Temperature Reactors	1
1.1.2 Fission Product Release	6
1.1.3 Aerosol Generation in VHTRs	6
1.1.4 The Advantages of Using Helium as a Coolant	7
1.2 Previous Work on Aerosol Deflection	7
1.3 Problem Statement	10
1.4 Objectives	10

1.5	The Scope Of Research	11
2	Theoretical Deflection Models	13
2.1	Introduction	13
2.2	Stochastic Deflection Model	14
2.2.1	Kinetic Theory of Gases	14
2.2.2	Mean Free Time	16
2.2.3	Elastic Collisions	17
2.2.4	Electrophoresis	20
2.2.5	Atomic and Molecular Polarizability	21
2.3	Deterministic Deflection Model	22
2.3.1	Dielectrophoresis	23
2.3.2	Momentum Transport Equation	29
3	Numerical Simulations	33
3.1	Stochastic Deflection Model	33
3.1.1	Numerical Method	33
3.1.2	Assumptions	34
3.1.3	Sample Calculations	34
3.2	Deterministic Deflection Model	39
3.2.1	Numerical Method	39
3.2.2	Assumptions	40
3.2.3	Sample Calculations	41

4	Results and Discussions	46
4.1	Stochastic Deflection Model	46
4.1.1	Electrophoresis	46
4.1.2	Dielectrophoresis	52
4.2	Deterministic Deflection Model	53
5	Discussions and Conclusions	58
5.1	Stochastic Deflection Model	58
5.1.1	Electrophoresis	58
5.1.2	Dielectrophoresis	60
5.2	Deterministic Deflection Model	61
A		69
A.1	Derivations From Basic Principles	69
A.1.1	Derivation of Flow Velocity Profile Equation	69
A.1.2	Terminal Velocity	72
A.1.3	Dielectrophoresis derivation	73
B		77
B.1	Numerical Programs and Flow Charts	77
B.2	Numerical Algorithm for Stochastic Model	77
B.3	Numerical Algorithm for Deterministic Model	79
C		81
C.1	Electrostatic Precipitation	81

C.1.1	Electrical Mobility	83
C.1.2	Slip Correction Factor	84
C.1.3	Electrophoresis Numerical Method	85
C.1.4	Assumptions	85
C.1.5	Results	86

List of Figures

1.1	The pebble bed reactor main power system (Mar04).	2
1.2	The prismatic block fuel assembly (Tak06).	3
1.3	High temperature fuel pebble containing approximately 1500 TRISO fuel particles (Sla04).	4
1.4	Cross section of the primary loop of the HTR-PM. 1 reactor core; 2 side reflector and carbon thermal shield; 3 core barrel; 4 reactor pressure vessel; 5 steam generator; 6 steam generator vessel; 7 coaxial gas duct; 8 water-cooling panel; 9 blower; 10 fuel discharging tube (Zuo09).	5
1.5	Photo-micrograph of a coated particle showing radiation induced micro-cracks on the coating layers (Pet03).	6
2.1	Schematic representation of the geometrical coordinate for the collision of silver and helium in an elastic collision.	19
2.2	Schematic representation of electrophoresis with a charged particle (A) and a neutral particle (B) in the uniform electric field.	20
2.3	(A) charged particle and (B) neutral particle under the influence of nonuniform electric fields (Lin07).	23
2.4	A schematic representation of two particle groups <i>A</i> and <i>B</i> deflected to different positions under the influence of dielectrophoresis, gravity and hydrodynamic velocity profile (Lin07).	27

2.5	A schematic representation to show the effects of negative- and positive-dielectrophoresis in a flow field (Lin07).	28
2.6	Equipotential field lines surrounding the nonuniform electrode structure made of a pin and plate configuration. The applied voltage at each electrode is $V = 1000$ volts	28
2.7	The schematic representation (a) the coordinate system and, (b) the free body force diagram.	29
3.1	A schematic representation of a velocity profile showing the forces acting on two particles (Lin07).	39
4.1	Helium velocity distributions: Figure (a) shows a comparison of the theoretical Maxwell-Boltzmann velocity distribution from eq. (2.10) normalized with respect to probable velocity (Temperature $T = 20^\circ$ C and pressure $P = 1$ atm), and the random velocities of helium atoms binned into a distribution. Figure (b) shows a comparison of randomly sampled helium velocity distributions, and the cumulative velocity distribution.	47
4.2	Comparison between Cronje results (broken lines) and values obtained from work done in this thesis (solid line) for the simulation time of $0.1 \mu\text{s}$: (a) the temperature is 20° C and the pressure is 1 bar, (b) the temperature is 900° C and the pressure is 90 bar.	50
4.3	Maxwellian velocity distribution for silver particles after collisions (a) random velocity distribution, and (b) theoretical distribution from eq. (2.10) for silver at $T = 20^\circ$ C and 1 atm.	51
4.4	Nonuniform electric field distribution on a nonsimilar electrode structure. Each arrow represents the amplitude and direction of the electric field at the center of its tail.	53

4.5	The trajectory of a silver particle (radius $3 \mu\text{m}$) deflected in a nonuniform electric field under the deterministic deflection model (using components of equation 2.60). The deflections start at an arbitrary location 1: (a) is a projection in the field plane with x - and z -components of the position; (b) is the x -component of the position varying with time; and (c) is z -components of the position varying with time. The numerical calculation time is $50.999 \mu\text{s}$. Note: x is the direction from one plate to the other and z is the direction across the plates.	56
4.6	The trajectory of a silver particle (radius $3 \mu\text{m}$) deflected in a nonuniform electric field under the deterministic deflection model (using components of equation 2.60). The deflections start from at an arbitrary location 2: (a) is a projection in the field plane with x - and z -components of the position; (b) is the x -component of the position varying with time; and (c) is z -components of the position varying with time. The numerical calculation time is $50.999 \mu\text{s}$. Note: x is the direction from one plate to the other and z is the direction across the plates.	57
A.1	The force balance on the fluid element to determine the velocity profile using two parallel plates.	70
A.2	Helium Poiseuille flow profile normalized by the average velocity (v_{flow}/v_{ave}) from eq. (A.12) between two infinite parallel plates. The height (h) of the parallel plates is 10 cm.	72
A.3	Spherical silver particle of radius R and permittivity ϵ_{Ag} immersed in helium and subjected to a uniform electric field (Jon95).	74
B.1	A schematic representation of the algorithm used in the stochastic numerical simulations.	78
B.2	A schematic representation of the algorithm used in the deterministic numerical calculations.	80
C.1	Two dimensional system of electrostatic precipitation.	83
C.2	The relationship between the total distance travelled in the x -direction (x is the direction of flow or motion) for a $3 \mu\text{m}$ charged particle and the total time taken to travel the distance, with an applied voltage of (a) 1 kV and (b) 2 kV. The helium bulk velocity is 0.012ms^{-1} and the height between the parallel plates is 10 cm.	87

List of Tables

2.1	Comparison of dielectrophoresis and electrophoresis (Lin07 and Poh58).	24
4.1	Deflection results from the stochastic simulations with pressure and temperature of 1 bar and 20 °C, respectively. The time that the particle spends without colliding is calculated in the simulations as a constant value of 0.189285 ns.	48
4.2	Deflection results from the stochastic simulations with pressure and temperature as 90 bar and 900 °C, respectively. The time that the particle spends without colliding is calculated in the simulations as a constant value of 0.004207 ns.	48
4.3	Deflection comparison between the simulations and results from Cronje (2007) and Steyn (2009). The results are compared for different temperature and pressure and for a predefined time of 0.1 μ s.	49
4.4	Particle deflection results for the deterministic deflection model with contributions from dielectrophoretic for a specific initial conditions. The single clustered silver particle with a size of 3 μ m. The numerical calculation time is 50.999 μ s.	54
A.1	Values of t_t for different particle radii using eq. (A.15). The density, ρ , of the particle is 10500 kg/m^{-3} , and the viscosity μ (of temperature 300 K and 1 atmosphere pressure) is $20.1 \times 10^{-6} \text{ kgms}^{-1}$	73

C.1 Electrostatic precipitation numerical results for a 3 μm charged particle. The helium bulk velocity is 0.012 ms^{-1} . The total deflection distance in the direction of the electric field is 10 cm. 86

Chapter 1

Introduction

Deflection of particles generated during normal operation of a reactor is an issue of great interest, particularly in Very High Temperature Reactors (VHTRs). This is because in the primary circuit components of VHTRs, various unwanted fission products such as Kr, Xe, I, Cs, Sr, and Ag are generated in the core and find their way into the helium coolant stream. The presence of radioactive particles in the primary circuit components cause an unwanted maintenance problem from a radiation hazard viewpoint. This section of the thesis provides a background on the importance of the research, the problem statements, the objectives of the work, and finally, the scope of the research.

1.1 Background

1.1.1 Very High Temperature Reactors

The Generation IV Very High Temperature Reactor (VHTR) is one of six nuclear reactor design concepts that have been identified as being able to ensure that future nuclear reactors provide sustainable energy to many of the industrialized and developing countries. The design is economically competitive, incorporates high levels of safety and reliability, includes proliferation resistance and physical protection against acts of terrorism. It is predicted that VHTRs will be ready for commercialization before the year 2030 by which

time many of the nuclear reactors currently existing will be at or near the end of their operating licensed

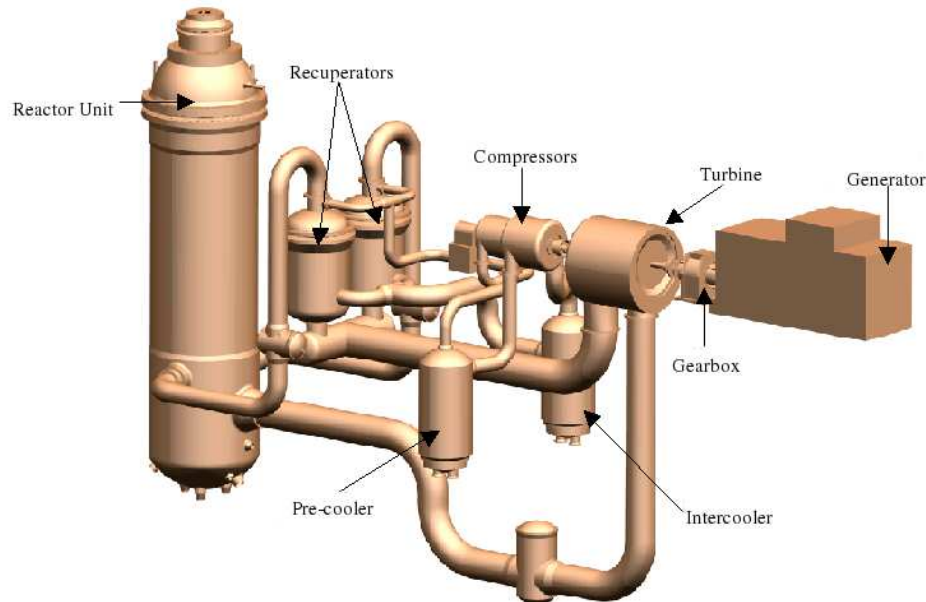


Figure 1.1: The pebble bed reactor main power system (Mar04).

lifetime (US02). VHTRs are graphite moderated, helium cooled reactors, and follow the work completed since the 1960s on high-temperature gas-cooled reactors (HTGRs) including the Dragon (Eve66), the Peach Bottom (Kin03), AVR (Cle85; Krü85), THTR (Roe90; Die97), and the Fort St. Vrain (Ful88) and the Chinese HTR10 (Zou09). It is attractive because of the capability to achieve operating temperatures up to 1000 °C. Therefore, it can generate electricity using gas turbines with high efficiency (> 50 %). The high operating temperatures would also allow the VHTR to be used for hydrogen production with high efficiency using thermochemical processes with or without co-generation of electricity (US02; Gho09).

The two popular reactor fuel core designs are the *pebble bed* and the *prismatic block*. Figure 1.1 shows the pebble bed module reactor main power system and figure 1.2 is a design of the prismatic block fuel assembly, while figure 1.3 shows a pebble design. Both the pebble bed and the prismatic block designs utilize tristructural isotropic (TRISO) fuel particles and each TRISO particle is approximately 1 mm in diameter contains a fissile kernel (i.e. UO_2 , UC_2). The fuel is surrounded by four protective coatings

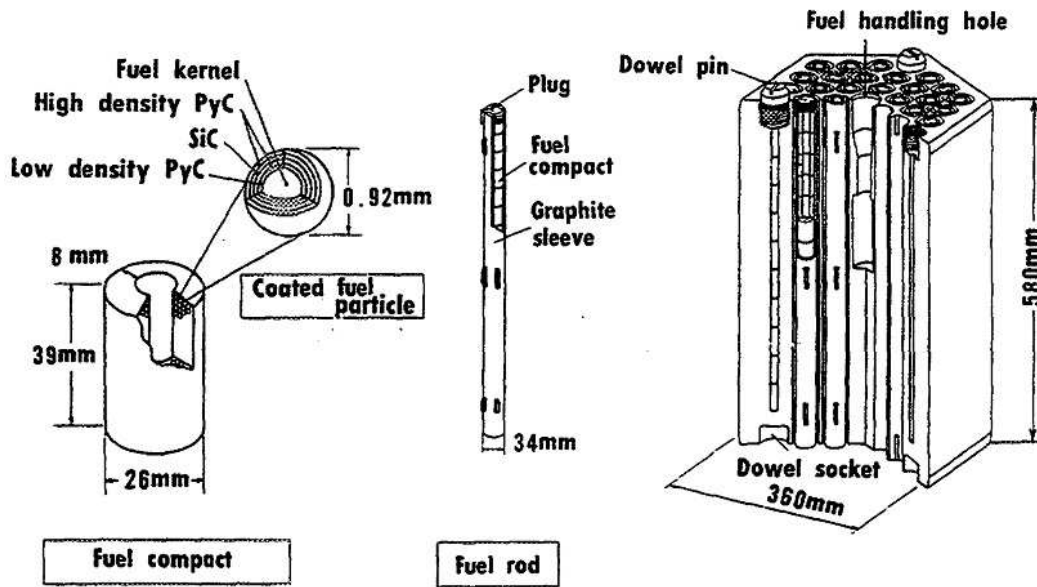


Figure 1.2: The prismatic block fuel assembly (Tak06).

designed to contain fission products and gases while providing thermal and structural support. Other fissile fuels such as spent light water reactor fuel, weapons surplus plutonium (Pu) or thorium (Th) may be used and would extend the capabilities of the TRISO fuel particle and help to reduce nuclear waste and proliferation (Ven05).

For the pebble bed design, the TRISO fuel particles are mixed with graphite powder and pressed into spheres or pebbles that are approximately 60 mm in diameter (as shown in figure 1.3). On the order of 360,000 pebbles, each containing approximately 11,000 TRISO fuel particles, are circulated through a reaction chamber (Ven05). The fuel is inserted at the top, consumed as they settle toward the bottom, and subsequently removed from the reactor (Kad05). The pebbles can be examined upon exiting the reaction chamber, checked for fuel consumption and defects, and recirculated as necessary.

In contrast, for the prismatic block design the TRISO fuel is mixed with graphite powder and pressed into a cylinder which is placed into a stationary arrangement within the reactor core (see figure 1.2). The main advantage of the pebble bed reactor is online refueling while the prismatic block design, like traditional nuclear reactor designs, requires the reactor to be shut down during refueling. Both reactors are promising

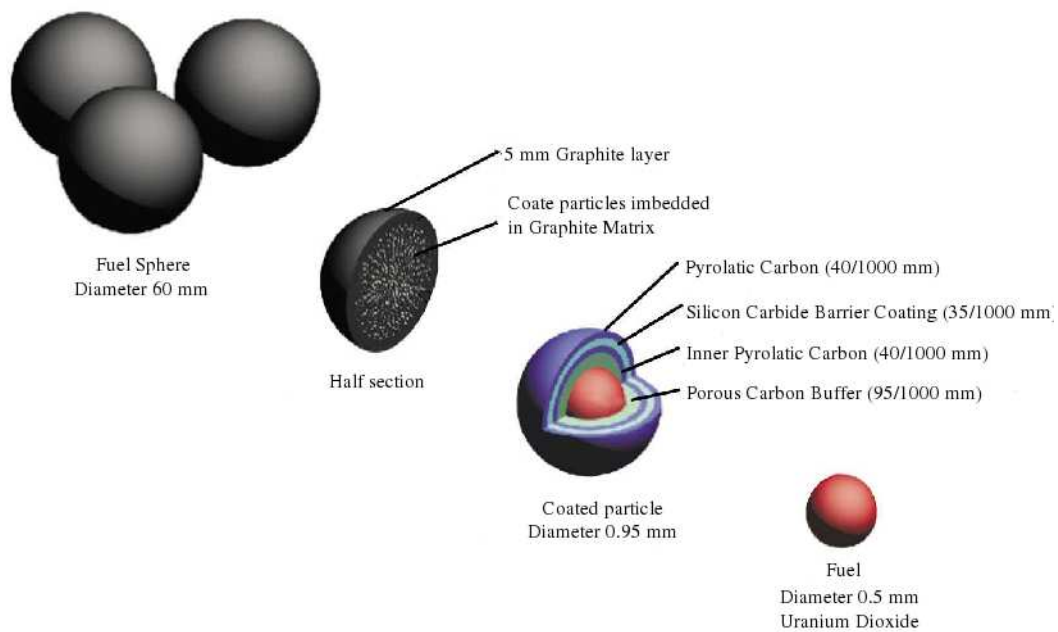


Figure 1.3: High temperature fuel pebble containing approximately 1500 TRISO fuel particles (Sla04).

as modular designs which would allow for variable plant capacity. This is because additional modules can be introduced at a later stage. Also, such reactors would reduce costs because they can be subassembled in a factory. The payback period can be reduced substantially by bringing the modules online as they are constructed. Of the two options the Chinese nuclear program has opted for the pebble bed reactor and at this time a full-scale demonstration plant is under construction (Zuo09). This demonstration plant is called the HTR-PM (high-temperature-reactor pebble-bed module) and follows the successful construction and operation of the 10MWth high-temperature gas-cooled test reactor (HTR-10) (Zuo09). The HTR-PM plant will consist of two nuclear steam supply system (NSSS), known as modules. Each one will comprise of a single zone 250MWth pebble-bed modular reactor and a steam generator. The two NSSS modules will feed one steam turbine and generate an electric power of 210MW. Figure 1.4 shows the cross-section of the HTR reactor building. A fuel production line, which is closely based on the technology of the HTR-10 fuel production line, will be built to fabricate 300,000 pebble fuel elements per year (Zuo09). It is envisaged that this plant will demonstrate the economic competitiveness of commercial HTRPM plants and show that

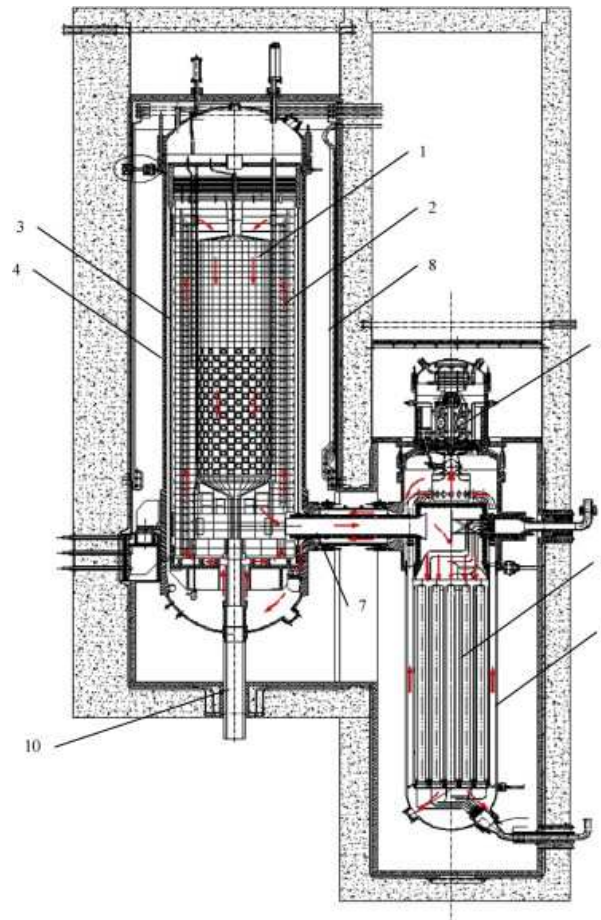


Figure 1.4: Cross section of the primary loop of the HTR-PM. 1 reactor core; 2 side reflector and carbon thermal shield; 3 core barrel; 4 reactor pressure vessel; 5 steam generator; 6 steam generator vessel; 7 coaxial gas duct; 8 water-cooling panel; 9 blower; 10 fuel discharging tube (Zuo09).

HTR-PM plants do not need accident management procedures because the reactor has a passive accident management, and there is no need for offsite emergency measures. According to the current schedule of the project the completion date of the demonstration plant will be around 2013 (Zuo09). As a generation IV reactor the HTR-PM project will play a critical role for the development of Generation-IV nuclear energy technologies. One concern with the pebble bed reactor is that of the release of fission products from the pebbles that are meant to act as containment of these materials during normal operation. The problem of fission product release is discussed in more detail in the next section.

1.1.2 Fission Product Release

TRISO fuel particles are designed to retain fission products and gases throughout their lifetime. However, some of the fission products are inevitably released because of the limitations in manufacturability, service failures, and the retention-performance of TRISO coatings towards certain isotopes. Figure 1.5 shows manufacturing defects leading to fission product release from TRISO fuel particles including cracked coatings and uranium contamination in the graphite. Manufacturing defects in the TRISO coatings may lead to cracking

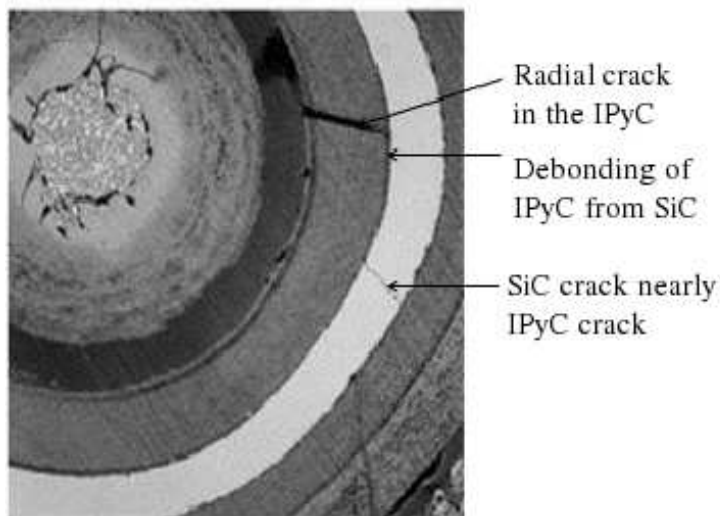


Figure 1.5: Photo-micrograph of a coated particle showing radiation induced micro-cracks on the coating layers (Pet03).

and failure of the Silicon Carbide (SiC) and/or Pyrolytic Carbon (PyC) layers during service. Such failures may expose the kernel and cause the release of fission gases, while failure of any layer will release fission metals (Wic91). During normal operation small quantities of graphite dust are found in the helium coolant due to abrasion of the pebbles in the reactor. Section 1.1.3 that follows discusses the generation of aerosols in VHTRs.

1.1.3 Aerosol Generation in VHTRs

One of the design challenges of the VHTR is that they produce aerosols during normal operation and in the event of an accident. Pebble bed reactors create graphite dust due to abrasion between pebbles as they

move through the reactor core. Inside the reactor core, the dust is lifted by the helium coolant creating a graphite aerosol which is carried throughout the cooling circuit and possibly into the gas turbines as in the AVR (Cle85). Various fission products also constitute a fraction of the aerosols within the reactor due to failure such as cracks or broken fuel particles and diffusion through TRISO coatings.

Dust accumulation can damage system components such as the gas turbine and also become a health hazard for personnel during plant maintenance (Ven05). Several accident scenarios such as air ingress (IAE97), water ingress (IAE97; Kug88), and depressurization (IAE97; Ste08; Wic91) may lead to the generation and release of aerosol and fission products from the reactor. Therefore, it is important to determine methods that would deflect these aerosol particles with the aim of removing them at the material containment surfaces. Helium is the driving flow of aerosol particles generated in VHTRs during normal operation. This is simply because it is used as a coolant. Some of the main reasons why helium is preferred as a coolant in the VHTRs are discussed in the next section 1.1.4.

1.1.4 The Advantages of Using Helium as a Coolant

The use of helium as a coolant gas is an advantage because it is chemically inert, and will not become radioactive while coming in contact with neutrons; only small amounts of hydrogen will be activated to form tritium. Helium has a high temperature potential therefore efficient heat transfer inside the reactor can be achieved. A high temperature allows the use of heat for other technological purposes such as the production of hydrogen from water (Pon03). Previously, work has been done to deflect dust generated in the reactor core and fission products released from the pebbles. Section 1.2 looks at some of the research and discusses the techniques that were used and a brief summary of the results that were obtained.

1.2 Previous Work on Aerosol Deflection

Radioactive aerosol particles may exist in a VHTR and there has been interest in minimizing radioactive contamination of the reactor coolant circuit due to these particles. The main candidate that has been identified as a cause for concern and the focus of research to minimizing radioactive contamination of the reactor

coolant circuit is silver. This is because the design of the coated particles limits the release of fission products into the coolant except for silver (Ag^{110m}). Ag^{110m} is a long lived metallic fission product formed inside the nuclear reactor core and is the only known element released out of the coated particles into the coolant at any temperature above 1150 °C when the reactor starts to heat up. The release occurs on intact coated particles, failed particles and also from defective particles (van04). The amount of released silver is initially small and occurs as the pebble heats up and this is strongly dependent on the temperature of the core (Sla04). It is therefore able to reach the surface of the reactor core and enter into the Helium coolant flowing throughout the reactor. Thus Ag^{110m} will be circulated through the reactor circuit until it reaches the cooler sides of the MPS where it will start to plate out.

Ag^{110m} has a relatively long half-life of 253 days and has two possible modes of decay to the Cd^{110} ground state and accompanied by gamma-ray emissions. The result is the contamination of the coolant and the MPS resulting in a radiation hazard to members of the public in case of loss of coolant accident conditions (LOCA) or to operating personnel when scheduled maintenance has to be done to the reactor. A number of studies that have been done to investigate the deflection of silver particles to the walls of the helium hot pipe are discussed in this section.

Cronje 2007 used the magnetic field force in a stochastic framework employing the kinetic theory of gases to deflect silver ions and atoms. In the work it was shown that using a magnetic field gives very small deflections. For example, an applied magnetic field of 0.0005 Tesla could only achieve a maximum deflection of 5×10^{-19} meters (Cro07). It was verified that a magnetic field on its own will not be able to deflect silver ions in helium. However, their test on using uniform electric fields (electrophoresis) to deflect silver ions showed promising results (see their results in chapter 4) and forms a point of departure for this work.

Cronje 2007 used the magnetic field force in a stochastic framework employing the kinetic theory of gases to deflect silver ions and atoms. In the work it was shown that using a magnetic field gives very small deflections. For example, an applied magnetic field of 0.0005 Tesla could only achieve a maximum deflection of 5×10^{-19} meters (Cro07). It was verified that a magnetic field on its own will not be able to deflect silver ions in helium. However, their test on using uniform electric fields (electrophoresis) to deflect silver ions showed promising results (see their results in chapter 4) and forms a point of departure for this work.

Another investigation was performed by Mokhantshang (2008). In the experiment, the PBMR-Magnetic Isotope Scrubber (MIS), which uses magnetic fields to deflect silver atoms was used. The theoretical calculations from that work used magnetic fields ranging from 0.125 to 4 Tesla producing forces ranging from 5.80×10^{-23} to 1.85×10^{-21} N, and obtained theoretical deflections ranging from 1 to 32 mm for silver atoms (Mok08). The work also revealed that shorter magnet lengths and closer target positions with respect to the silver generation oven exit of the experiment gives less or no deflections. The suggestion made then was an increase in the distance of the target from the oven exit, and the use of longer magnet lengths to subject silver atoms to a magnetic force over a long distance (e.g. 93 meters). However, the helium hot pipe in a VHTR such as PBMR design is approximately 6 meters and Mokhantshang determined that the magnetic field is ineffective for distances less than 93 meters (Mok08). Therefore, the magnetic field was not an appropriate option in deflecting silver atoms in the VHTR.

Kheswa (2011) used magnetic fields in an experiment to deflect silver-109 atoms using permanent magnets. A magnetic circuit capable of producing a homogeneous and inhomogeneous magnetic fields was used. The experimental work for the deflection of the Ag-atoms with the roundhole collimators of 1 mm diameter showed that inhomogeneous magnetic fields increased the width of the deposited silver atoms on the target by 3.9 mm and 5.54 mm. This was observed when the target was positioned 13 mm and 30 mm away from the magnets, respectively (Khe11). The deflections were 1.95 mm when the target plate was positioned 13 mm away from the magnet, which is 3.17 % greater than the theoretical deflection of 1.89 mm calculated for the atoms speed of 43 ms^{-1} . The deflection distance was 2.88 mm when the target plate was positioned 30 mm away from the magnet, which is 4.86 % greater than the theoretical deflection value of 2.74 mm calculated at atoms speed of 43 ms^{-1} (Khe11). The deflection of silver atoms was then collimated with a pair of slits and the target plate was positioned at 13 mm away from the magnet. This produced the maximum deflections of 1.27 mm in the positive and negative z direction (2.42 % greater than the theoretical value, 1.24 mm, calculated for an atom speed of 53 ms^{-1} and target plate positioned 13 mm away from the magnet). In the positive and negative x direction the value was 1.25 (0.81 % greater than the theoretical value, 1.24 mm, calculated for atoms speed of 53 ms^{-1}), (Khe11).

It was concluded that, although the results were representative of the Stern-Gerlach experiment the tech-

nique was not effective in removing silver atoms from the helium stream. This is because the inhomogeneous magnetic field was unable to split the beam of silver atoms into two separate beams in vacuum (1.33×10^{-5} mbar). Hence it would have been even more difficult to split the beam of silver atoms in helium, due to the silver atoms having a shorter mean free path in helium compared to vacuum (Khe11).

The work done in this research is motivated by recommendations from the works discussed above, that uniform electric fields have a potential in deflecting aerosol particle such as that of silver. The next section 1.3 that follows provides the problem statement.

1.3 Problem Statement

For the design of future VHTR, and also for accurate accident modelling, the knowledge of particle deflections to the reactor system walls using deflecting techniques, such as, electric fields, magnetic fields and centrifugal force to deflect graphite and fission products is very important. The present research investigates dielectrophoresis (deterministic method) and electrophoresis (stochastic method) as suitable methods for deflecting aerosols. The reason is that dielectrophoresis produces nanorange velocities as a result is overshadowed by Brownian motion (see chapter 4 section 5.1.2). This work will specifically examine how well the dielectrophoresis and electrophoresis techniques perform in deflecting aerosol silver particles released during normal operation in the reactor core. The success of the work done in this research is measured by the achievement of the objectives that are outlined in the following section 1.4.

1.4 Objectives

The development of the complete solution is measured by assigning objectives with their achievement giving the complete solution to the proposed problem in this research. These are listed as follows:

1. Develop and test a stochastic Monte Carlo simulation algorithm to determine the deflection of silver ions in a helium gas using uniform electric fields (electrophoresis).
2. Test the deflection of silver atoms using the polarizability of an atom from nonuniform electric fields

and compare the movement obtained with the Brownian motion.

3. Develop and test a deterministic numerical algorithm and use it to predict silver particle deflections in a helium medium using dielectrophoresis (nonuniform electric field).
4. Obtain the helium velocity profile for laminar flow and include its contribution in the deterministic deflection model algorithm.
5. Perform sample calculations to show the procedure followed in the algorithms and the values produced.
6. Compare the results from the stochastic deflection model with those from other works.
7. Discuss the feasibility of dielectrophoresis and electrophoresis as appropriate options for deflecting silver particles.

In this work a particle will be used often to mean a silver atom, silver ion or micronsize cluster. The scope of research is given in section 1.5 and provides the structure of the thesis.

1.5 The Scope Of Research

Chapter 1 provides the background by discussing the research problem and the reasons behind the need for data on the deflection of particles in a helium medium. A summary of the most recent studies and their findings is given to further support motivation for this work. The problem statement and the scope of research are given. Chapter 2 gives the theoretical construction of the deflection models, namely the stochastic and deterministic deflection models used to obtain the objectives of this work. A stochastic deflection model is developed using kinetic theory of gases and statistical methods. Chapter 3 gives the numerical simulations required for both the stochastic and deterministic deflection models by focussing on the numerical methods and the assumptions made. In this chapter the sample calculations have also been included.

Chapter 4 presents and discusses the results obtained using the deflection models developed in chapter 2 and their respective numerical simulations constructed in chapter 3. It also compares the results with those from previous research. Finally, Chapter 5 presents a brief summary of the conclusions and gives recommendations. Appendices A, B and C show the derivation, from basic principles, of equations used in the

calculations, the numerical programs and flow chart, and a deflection model based on the electrostatic precipitation, respectively.

Chapter 2

Theoretical Deflection Models

2.1 Introduction

This chapter considers and develops two different deflection models for the deflection of silver particles in a helium flow. The two models proposed are namely, the stochastic and deterministic deflection models. The first deflection model (stochastic) is governed by the probability of collisions. It describes the motion of a single ion or atom as it collides with helium atoms. The forces used are due to the electrostatic potential of an ion or the polarizability of an atom.

The second deflection model (deterministic), is governed by equations of state, Coulombic and dielectrophoretic forces. This deflection model describes the deflection of microparticles in a continuum of a helium flow medium. The model is simplified by selecting a particle and studying its trajectory as it is deflected in the electric field, ignoring its interactions (which may cause chemical reactions) with other particles within the bulk of the system, and taking into account gravity and viscous effects.

2.2 Stochastic Deflection Model

The stochastic deflection model describes the random movement of a single silver particle during collisions with helium gas atoms. It is a two-dimensional model motivated by the work done by Cronje (Cro07). In the model, the assumption is that the collisions are elastic, implying that the energy is only exchanged as translational kinetic energy (How65). The model is used to determine the deflection of silver ion nanoparticle in a uniform electric field.

Molecules in suspension are constantly in random motion as they collide with other molecules around them (Sea64), and this mechanism is called *Brownian motion*. In this work, a force, $\mathbf{F}_{applied}$, due to uniform electric fields is applied between these collisions resulting in the acceleration of the silver particle. The applied force can be a combination of the Coulombic force (\mathbf{F}_{ES}), the dielectrophoretic force (\mathbf{F}_{DEP}) given as

$$\mathbf{F}_{applied} = \mathbf{F}_{ES} + \mathbf{F}_{DEP}. \quad (2.1)$$

In eq. (2.1), the gravitational force is ignored and the hydrodynamic drag force is incorporated within the random velocities of the helium atom. The stochastic deflection model is based on elastic collisions of particles, therefore to certify the velocity of helium atoms to complete the momentum transfer calculations it is necessary to discuss the speed distribution of the helium-silver gas in the next section.

2.2.1 Kinetic Theory of Gases

The *ideal* gas law is an appropriate point to start the development of the model to be used in this work. It provides the relationship between pressure P , volume V , absolute temperature T and the number of moles n of the gas (Sea64). The *ideal* gas law equation is given as

$$PV = nRT = Nk_B T, \quad (2.2)$$

where n is the number of moles, R is the universal gas constant and k_B is the Boltzmann constant. A mole of any material will contain an Avogadro's number of molecules. Thus, the number of molecules per volume

can be determined as

$$N_m = \frac{nN_A}{V}. \quad (2.3)$$

Eq. (2.2) can be rewritten as $n = \frac{PV}{RT}$. Inserting this into eq. (2.3) gives

$$N_m = \frac{N_A P}{RT}. \quad (2.4)$$

The volumes cancel each other out and $\frac{R}{N_A}$ can be replaced by k_B , such that eq. (2.4) becomes

$$N_m = \frac{P}{k_B T}. \quad (2.5)$$

The speed distribution $f(v)$ of the particles, which is a statistical density function, can be expressed by a Maxwell-Boltzmann velocity distribution function (Sea64) which, for the molecules of an ideal gas, is given by

$$f(v) = 4\pi \left\{ \frac{M}{2\pi RT} \right\}^{3/2} v^2 \exp \left\{ \frac{-Mv^2}{2RT} \right\}, \quad (2.6)$$

where M is molar mass. There are a number of quantities of interest such as the most probable speed, v_p , mean speed, \bar{v} , and root mean speed, v_{rms} , that can be calculated from the velocity function. These quantities are given as

$$v_p = \sqrt{\frac{2RT}{M}}, \quad (2.7)$$

$$\bar{v} = \sqrt{\frac{8RT}{\pi M}}, \quad (2.8)$$

$$v_{rms} = \sqrt{\frac{3RT}{M}}. \quad (2.9)$$

The values for the most probable speed, the mean speed, and the root mean speed at 20 °C and 1 bar for silver are 213.4433, 240.845 and 261.4136 ms⁻¹, respectively. For helium at the same temperature and pressure, these values are 1103.937, 1245.66 and 1352.042 ms⁻¹, respectively. In the case of 900 °C and 90 bar, the values are 426.987, 481.803 and 522.950 ms⁻¹ for silver and 2208.393, 2491.904 and 2704.717 ms⁻¹ for helium. When the most probable speed eq. (2.7) is inserted into eq. (2.6), the resulting expression for

the velocity distribution is

$$f(v') = \frac{4}{\sqrt{\pi}v_p} \left\{ \frac{v}{v_p} \right\}^2 \exp \left\{ -\frac{v^2}{v_p^2} \right\}. \quad (2.10)$$

where v' is the velocity normalized by the probable velocity (e.g. $\frac{v}{v_p}$). The mean free time is the between successive collisions in a gas. This quantity can be estimated from kinetic theory of gases. The next section derives the equation for the mean free time, discusses the quantity and presents theoretical values calculated from the derived expressions.

2.2.2 Mean Free Time

The mean free time between collisions in a gas can be estimated from kinetic theory by considering an atom of silver Ag with diameter d_{Ag} moving through a gas of helium atoms He having diameter d_{He} . Assuming that the gas consists of mostly He atoms with only a very small fraction of Ag atoms. The collisions between Ag atoms can be ignored. The effective collision cross-section is the area with radius r given by

$$\begin{aligned} A &= \pi r^2, \\ r &= \frac{d_{Ag} + d_{He}}{2}, \end{aligned} \quad (2.11)$$

where diameter values, d_{He} and d_{Ag} , for helium and silver are 0.098 nm and 0.35 nm, respectively (Cro07).

The mean free time, τ , is the elapsed time between successive collisions, averaged over the speed distribution of the atoms and is given as

$$\begin{aligned} \tau &= \frac{R}{\pi r^2 N_A} \sqrt{\frac{m_{He}}{m_{Ag} + m_{He}}} \frac{1}{v_{Ag}} \frac{T}{P}, \\ v_{Ag} &= \sqrt{\frac{8k_B T}{\pi m_{Ag}}}. \end{aligned} \quad (2.12)$$

where v_{Ag} is the velocity of silver, while m_{Ag} and m_{He} are the masses of silver and helium, respectively.

Eq. (2.12) can be summarized into a useful expression for calculations by using the values for universal gas

constants R , Boltzmann's constant k_B , Avogadro's number N_A , and other constants as

$$\begin{aligned}\tau &= 0.043373 \frac{T}{r_{nm}^2 P_{atm}} \sqrt{\frac{m_{He}}{m_{Ag} + m_{He}}} \frac{1}{v_{Ag}}, \\ v_{Ag} &= 145.50842 \sqrt{\frac{T}{m_{Ag}}}.\end{aligned}\quad (2.13)$$

where r_{nm} is the effective collision cross-section and P_{atm} is given in atmospheric units. The mean free path λ can then be approximated by using the mean free time eq. (2.13) and the silver probable velocity v_{Ag} as

$$\lambda = \tau v_{Ag} = 0.043373 \frac{T}{r_{nm}^2 P_{atm}} \sqrt{\frac{m_{He}}{m_{Ag} + m_{He}}}.\quad (2.14)$$

The theoretical values for the mean free time τ and mean free path λ can be calculated using eq. (2.13) and 2.14. At a temperature of 20° C and a pressure of 1 atm the values for τ and λ are 0.2 ns and 47.4 nm, respectively. While at 900° C and a pressure of 90 atm the calculated values for τ and λ are approximately 0.0044 ns and 2.1 nm.

When a particle is deflected by an electric field force within a gas in a stochastic model, it experiences collisions with the gas atoms. The type of collisions considered here are elastic where momentum and energy are conserved. The velocity of the helium atoms in the helium hot pipe is 120 ms⁻¹ giving a kinetic energy of $0.5 \times (4/3)\pi(0.098 \times 10^{-9} \text{meters}/2)^3 \times 4.232 \text{kg/m}^3 \times (120 \text{ms}^{-1})^2 = 15.02 \times 10^{-27}$. This value is very small for the collisions to be considered non-relativistic collisions. The following section discusses the development of elastic collisions between silver and helium while providing the relevant equations (e.g. conservation of momentum and energy).

2.2.3 Elastic Collisions

It is essential to develop elastic collision equations between silver (Ag) ions and helium (He) atoms with mass m_{He} and m_{Ag} to be used in this work. Here, the starting point is the conservation of momentum and energy from which it is known that in any elastic collision momentum can be transferred at impact only and along the line connecting the center of the two particles. All other momentum components perpendicular

to this line are preserved resulting in elastic collisions in a centerline. If the respective velocities are given by v'_{He} and v'_{Ag} before collision, and V'_{He} and V'_{Ag} after collision, then the conservation of momentum and energy equations are given as

$$m_{He}v'_{He} + m_{Ag}v'_{Ag} = m_{He}V'_{He} + m_{Ag}V'_{Ag}. \quad (2.15)$$

$$\frac{1}{2}m_{He}v'^2_{He} + \frac{1}{2}m_{Ag}v'^2_{Ag} = \frac{1}{2}m_{He}V'^2_{He} + \frac{1}{2}m_{Ag}V'^2_{Ag}. \quad (2.16)$$

Transforming into a system where Ag is at rest before the collision gives

$$u'_{He} = v'_{He} - v'_{Ag}. \quad (2.17)$$

$$u'_{Ag} = v'_{Ag} - v'_{Ag} = 0. \quad (2.18)$$

$$U'_{He} = V'_{He} - v'_{Ag}. \quad (2.19)$$

$$U'_{Ag} = V'_{Ag} - v'_{Ag} = 0. \quad (2.20)$$

The transformations above are then substituted into the conservation eq. (2.15) and (2.16) to get the conservation equations in the system where Ag is at rest as

$$m_{He}u'_{He} = m_{He}U'_{He} + m_{Ag}U'_{Ag}. \quad (2.21)$$

$$\frac{1}{2}m_{He}u'^2_{He} = \frac{1}{2}m_{He}U'^2_{He} + \frac{1}{2}m_{Ag}U'^2_{Ag}. \quad (2.22)$$

Using eq. (2.21) and (2.22) the relative velocity of silver after collision can be obtained as

$$U'_{Ag} = \frac{2m_{He}}{m_{He} + m_{Ag}}u'_{He}. \quad (2.23)$$

It is necessary to transform back to the laboratory system in order to obtain the absolute velocities after the collision. Therefore, the velocities for silver and helium relative to silver before collision can be written as

$$\mathbf{V}_{He} = \mathbf{U}_{He} + v_{Ag}. \quad (2.24)$$

$$\mathbf{V}_{Ag} = \mathbf{U}_{Ag} + v_{Ag}. \quad (2.25)$$

The incident angle ψ of the velocity of He as defined in figure 2.1, can be calculated by

$$\psi = \arctan2(u_{He,y}, u_{He,x}), \quad (2.26)$$

where $u_{He,x}$ and $u_{He,y}$ are the x and y components of \mathbf{u}_{He} . If the impact plane is taken to be perpendicular to \mathbf{u}_{He} , Ag would experience more collisions on the side of the particle in the direction which it is moving. The phenomenon will produce a resistance to movement, namely, the drag force (Cro07). Helium collides with silver at an angle α , which is the angle between the incident \mathbf{u}_{He} and the centerline connecting the two particles. Angle α is calculated by choosing a collision radius ($-c < r < c$, where c is the distance between the two particles centres) and is given as

$$\alpha = \arcsin\left(\frac{r}{c}\right). \quad (2.27)$$

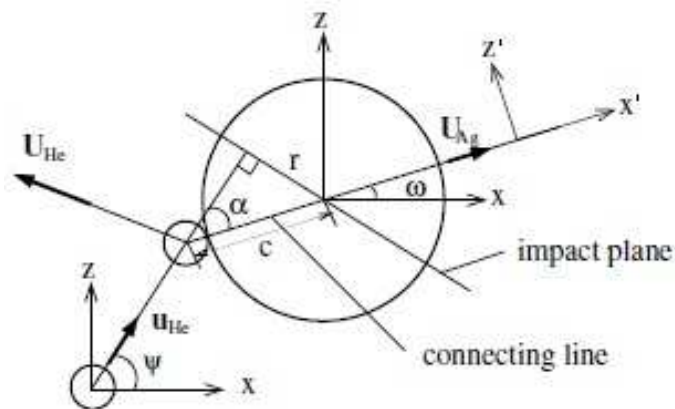


Figure 2.1: Schematic representation of the geometrical coordinate for the collision of silver and helium in an elastic collision.

Momentum is transferred only through the centerline connecting the two particles, and the velocity of the helium used in the one dimensional calculations of the silver is taken as $u_{He}\cos(\alpha)$. The development above considers a silver ion particle moving in a helium gas and deflected by a uniform electric field. However, a silver atom cannot be deflected by a uniform electric field. The force that will be used to act on the particle between collisions is the electrophoretic force or the electrostatic force, which uses a uniform electric field to deflect a particle is discussed in the next section.

2.2.4 Electrophoresis

The electrophoresis follows the principal that opposite charges attract and similar charges repel. The particle is required to be positively charged to move along the direction of the electric field lines to the negative electrode (Poh78 and Pet96). Figure 2.2 shows schematic representation of the effects of electrophoresis on a charged and a neutral particle. The principle behind electrophoretic force is the same as the electrostatic

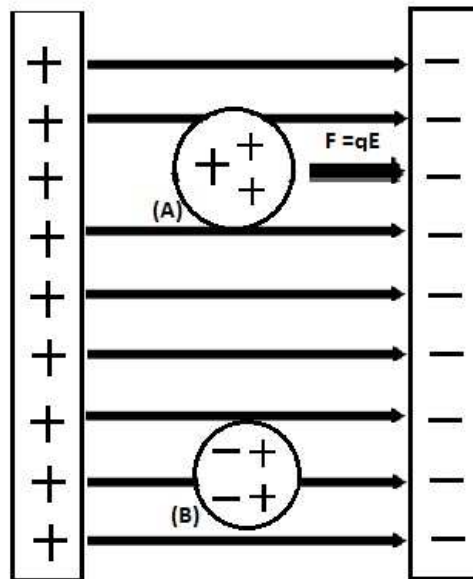


Figure 2.2: Schematic representation of electrophoresis with a charged particle (A) and a neutral particle (B) in the uniform electric field.

or Coulombic force and can be expressed as (Tay94)

$$\mathbf{F}_{ES} = q\mathbf{E} = -ne\mathbf{E}. \quad (2.28)$$

where \mathbf{F}_{ES} is the electrostatic force, n is the charge particle fraction, e is the electron charge 1.62×10^{-19} C, and \mathbf{E} is the electric field strength (V/m) and q is the particle charge. The change in the velocity $d\mathbf{v}_{Ag}$ of the silver particle due to the uniform electric force \mathbf{F}_{ES} after each collision in the stochastic deflection model is given as

$$m_{Ag}\mathbf{a} = q\mathbf{E} = -ne\mathbf{E}, \quad (2.29)$$

$$m \frac{d\mathbf{v}_{Ag}}{dt} = -ne\mathbf{E}, \quad (2.30)$$

$$d\mathbf{v}_{Ag} = \frac{-ne}{m_{Ag}} dt. \quad (2.31)$$

where m_{Ag} is the mass of silver particle, $d\mathbf{v}_{Ag}$ is the change in velocity of the silver particle due to the electric field and dt is the mean free time. The investigation of deflecting a silver atom is done by subjecting the particle to a nonhomogeneous electric field such that it experiences a force due to polarizability of the particle. The following section below discusses atomic and molecular polarizability.

2.2.5 Atomic and Molecular Polarizability

Dielectrophoresis (discussed later in the deterministic deflection model) is only applicable to particles in the range of $1 \mu\text{m}$ to 1mm in diameter (Jon95). The polarizability describes the response of the electron cloud in a particle to an electric field. Therefore, atoms and molecules smaller than $1 \mu\text{m}$ can be polarized. The dipole moment μ of an isolated particle (Hoo96) is given as

$$\mu = \alpha\mathbf{E}, \quad (2.32)$$

where \mathbf{E} is the electric field. Permanent electric dipole moments μ as a result of molecules without centres of symmetry (Hoo96). As the number of random collisions per unit time increase in temperature the tendency of the dipoles to line up with the electric field decreases and this decreases the influence of μ . This influence is seen in the total polarizability (Moo57), given as

$$\alpha = \alpha_{at} + \frac{\mu^2}{3k_B T}. \quad (2.33)$$

Pereiro and Baldomir (2007) determined the mean static polarizability per atom α_{at} in eq. (2.33) and found the permanent electric dipole moment to be negligible for silver clusters of up to 23 atoms (Per07). It was stated by Lide (1996) that electric dipole polarizability is constant for different electric fields (Lid96). Hence, an atom in a nonhomogeneous electric field experiences a force similar to that produced from dielectrophoresis. Using μ in eq. (2.32) and as created by the electric field an approximation for the dielectrophoretic force called the *dielectrophoretic approximation* (Jon95) can be written for the polarizability force of an atom as

$$\mathbf{F}_\alpha = \mathbf{m} \times \nabla \mathbf{E}. \quad (2.34)$$

The stochastic model developed above is a statistical simulation of the behavior of a silver ion in the nanorange size moving in a helium gas at specified temperature, pressure and initial conditions. In contrast, the deterministic model selects a single particle and using a discrete time stepping method studies its trajectory as it is deflected by the electric field force. The model is introduced in the following section.

2.3 Deterministic Deflection Model

The deterministic deflection model that is developed allows one to study the effects of an externally applied electric field on a charged or uncharged microparticle moving in a medium. The model uses two techniques, namely Electrophoresis (uniform electric fields) and dielectrophoresis (nonuniform electric fields).

2.3.1 Dielectrophoresis

Modern particle separation, deflection and transportation has been fundamental in many advances like cell biology and molecular genetics (Wan00). In the early years of using dielectrophoresis (*DEP*) techniques for deflecting, separating and transporting particles, macro-electrodes and channels were used (Fee81). This technique has been widely used to deflect particles in hydrodynamic microchannels (Min09). Dielectrophoresis is the translational motion of a neutral particle caused by polarization effects in a nonuniform electric field (Poh78). A neutral particle experiencing a positive dielectrophoretic force moves towards regions of high electric field strengths, and to regions of low electric field strength when experiencing negative dielectrophoresis, regardless of the electric field polarity (Mih06). In fact, both direct current (*DC*) and alternating current (*AC*) electric fields can be used to induce dielectrophoresis.

In this work, a dielectrophoresis technique can be used to separate silver from helium in a nonuniform electric field. This separation is guaranteed by the fact that there is a difference in permittivity, conductivity and particle size between silver and the helium. The nonuniform electric field gives the technique its ability to deflect, separate and transport charged and uncharged microparticles, respectively. Figure 2.3 illustrates the

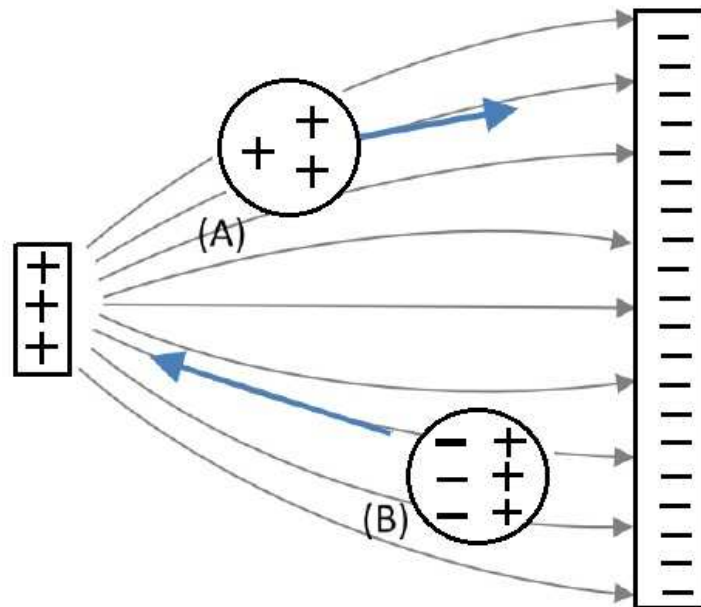


Figure 2.3: (A) charged particle and (B) neutral particle under the influence of nonuniform electric fields (Lin07).

effects of dielectrophoresis on both charged and neutral particles. A positively charged particle (A) under dielectrophoresis will move towards the negative electrode in the direction of the electric field lines. However, a neutral particle (B) under positive dielectrophoresis moves towards regions of high electric field strength located near the edges of the small electrode. Table 2.1 compares dielectrophoresis and electrophoresis in categories such as particle type, particle size, direction of motion, and field characteristics.

All particles exhibit *dielectrophoretic activity* in the presence of electric fields. However, the strength of the force depends on the medium and the electrical properties of the particle, the shape and size of the particle and the nonuniform electric field, and other characteristics of dielectrophoresis are given as:

- Dielectrophoretic force is seen only when a particle is in a nonuniform electric field.
- The force is independent of the polarity of the electric field, therefore, the phenomenon can be observed with both direct and alternating current excitation.
- The particles are attracted to regions of stronger electric field when they experience positive dielectrophoresis and to regions of weaker electric field when experiencing negative dielectrophoresis.
- Dielectrophoresis is most readily observed for particles with diameters ranging from approximately 1 to 1000 μm . Above 1000 μm , gravity and below 1 μm , Brownian motion overshadows the dielectrophoretic force.

Table 2.1: Comparison of dielectrophoresis and electrophoresis (Lin07 and Poh58).

Categories	Dielectrophoresis	Electrophoresis
Particle	Dielectric neutral particle	Particle with excessive charge
Particle size	Micron and submicron	Any molecular size
Direction of motion	Toward regions of highest field strength or regions of lowest field strength	Dependent on the direction of the field
Type of electric fields	Nonuniform	Uniform and Nonuniform
Medium	Medium must have a different dielectric constant than the particle	Medium could have the similar dielectric constant as the particle
Field strength	Must have high electric field strength	Use relatively low voltages
Field characteristics	Both direct and alternating electric fields	Direct current, no net movement under alternating electric fields

The dielectrophoretic force path can be developed by starting with a dielectric particle subjected to an electric field such that it is polarized. The polarization of a dielectric sphere by static homogeneous field is discussed in the following section.

Polarization of Dielectric Sphere by Static Homogeneous Field

When a dielectric particle is subjected to an electric field it will be polarized, to a certain extent. The dipoles in the particle will tend to align themselves with the electric field. The total electric field, \mathbf{E}_{res} , is then the difference of the original field, \mathbf{E} , and the field generated by the induced dipole, \mathbf{E}_{pol} (Jac75; Jon95). When the homogeneous linear dielectric sphere in a dielectric fluid is subjected to a homogeneous electric field, then \mathbf{E}_{res} can be calculated analytically and from basic principles for simple geometries as done in appendix A.1.3 derivations (Jac75; Jon95).

When a dielectric sphere is placed in a homogeneous electric field, \mathbf{E}_{hom} , it is polarized in such a manner that the electric dipole, \mathbf{E}_{pol} , generated by this polarization corresponds exactly to the electric field from an electric dipole, \mathbf{p} , placed at the center of the sphere given by

$$\mathbf{p} = 4\pi\epsilon_{he}r^3 \frac{\epsilon_{Ag} - \epsilon_{He}}{\epsilon_{Ag} + 2\epsilon_{He}} \mathbf{E}_{hom}, \quad (2.35)$$

where ϵ_{Ag} and ϵ_{He} are the permittivity of the silver particle and the surrounding helium medium, and r is the radius of the particle (Jac75; Jon95). Eq. (2.35) is a simple result for the dipole moment of a dielectric sphere in a homogeneous field. The next section treats the particle as a dipole and provides a formulation of the force exerted on the particle by the electric field, the *dielectrophoretic-force*.

Dielectrophoretic Force on Small Particle

A simple result for the dipole moment of a dielectric sphere in a homogeneous field as given by eq. (2.35) allows a treatment of the particle as a dipole when calculating the force exerted on the particle by the electric

field. The force, \mathbf{F}_{dip} , on a dipole in a field, \mathbf{E} , is

$$\mathbf{F}_{dip} = (\mathbf{p}\nabla)\mathbf{E}. \quad (2.36)$$

A non-zero gradient in the electric field is required for a net force to exist on the dipole. However, this is in violation of the assumption of field homogeneity under which \mathbf{p} was calculated in eq. (2.36). But if the particle radius r is much smaller than the characteristic distance d over which \mathbf{E} varies, i.e. $r \ll d$, then the particle will within its near vicinity experience a field which is largely homogeneous. Then the application of eq. (2.36) even in an inhomogeneous field can be justified. The force on the particle is referred to as the dielectrophoretic force, \mathbf{F}_{DEP} , given as

$$\mathbf{F}_{DEP} = 4\pi\epsilon_{He} \frac{\epsilon_{Ag} - \epsilon_{He}}{\epsilon_{Ag} + 2\epsilon_{He}} r^3 \mathbf{E}\nabla\mathbf{E}. \quad (2.37)$$

Eq. (2.37) is modified using the vector identity $\nabla(\mathbf{A}\cdot\mathbf{B}) = (\mathbf{A}\cdot\nabla)\mathbf{B} + (\mathbf{B}\cdot\nabla)\mathbf{A} + \mathbf{B}\times(\nabla\times\mathbf{A}) + \mathbf{A}\times(\nabla\times\mathbf{B})$ and $\nabla\times\mathbf{E} = 0$ (\mathbf{E} is an irrotational field) and rewritten (Min09) as

$$\mathbf{F}_{DEP} = 2\pi\epsilon_{He} \frac{\epsilon_{Ag} - \epsilon_{He}}{\epsilon_{Ag} + 2\epsilon_{He}} r^3 \nabla\mathbf{E}^2. \quad (2.38)$$

The electric field in eq. (2.38) appears as a squared quantity meaning that the direction of E has no significance for the direction of the DEP-force, \mathbf{F}_{DEP} . This factor plays a fundamental role in driving the dielectrophoretic force and it is dependent on the geometry of the electrodes. Eq. (2.38) can be summarized as follows

$$\mathbf{F}_{DEP} = 2\pi\epsilon_{He} K_{CM} a^3 \nabla\mathbf{E}^2, \quad (2.39)$$

where K_{CM} is called the Clausius-Mossotti factor (Poh78) given as

$$K_{CM} = \frac{\epsilon_{Ag} - \epsilon_{He}}{\epsilon_{Ag} + 2\epsilon_{He}}. \quad (2.40)$$

The factor, K_{CM} , (Jon95) can be rewritten in terms of the thermal conductivities (W/mK) of the silver particle (σ_{Ag}) and the helium medium σ_{He} as follows

$$K_{CM} = \frac{\sigma_{Ag} - \sigma_{He}}{\sigma_{Ag} + 2\sigma_{He}}, \quad (2.41)$$

What determines the direction of the DEP force is the gradient of the field and the sign of Clausius-Mossotti factor. If $K < 0$, the particle will be repelled by areas of high field gradient and this is termed *negative dielectrophoresis* or *nDEP*. If $K > 0$, the particle will be attracted to areas of higher field and termed *positive dielectrophoresis* or *pDEP* (Hua91). The dielectrophoretic force developed above is the fundamental driving force in deflecting particles using *dielectrophoresis*.

Nonuniform Electric Field

Nonuniform electric fields in this work depend on the nonsimilar electrodes. In figure 2.4 particles *A* and *B* are deflected to different positions by the electrophoretic force because of their difference in size. Also, in figure 2.5, a schematic representation of the flow with two different size particles shows that two particles under both positive and negative dielectrophoresis effects can be deflected independently. Moreover, the larger the particle the greater the deflection distance. A two-dimensional configuration of electrodes used in this work is shown in figure 2.6. The field simulator used to determine the nonuniform electric field is the

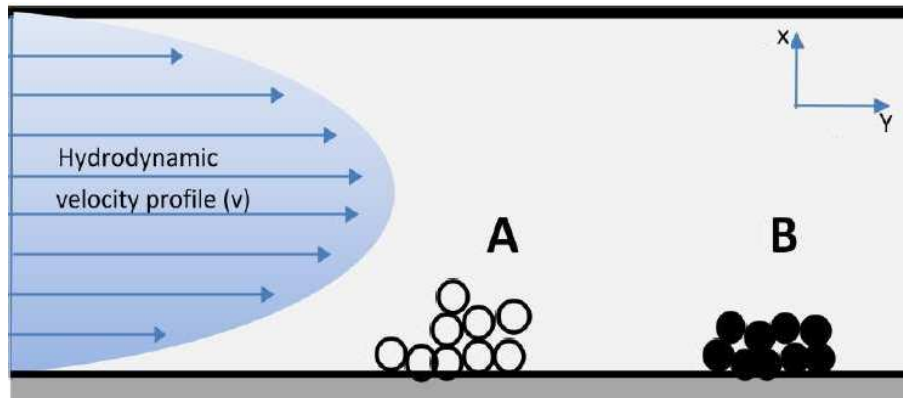


Figure 2.4: A schematic representation of two particle groups *A* and *B* deflected to different positions under the influence of dielectrophoresis, gravity and hydrodynamic velocity profile (Lin07).

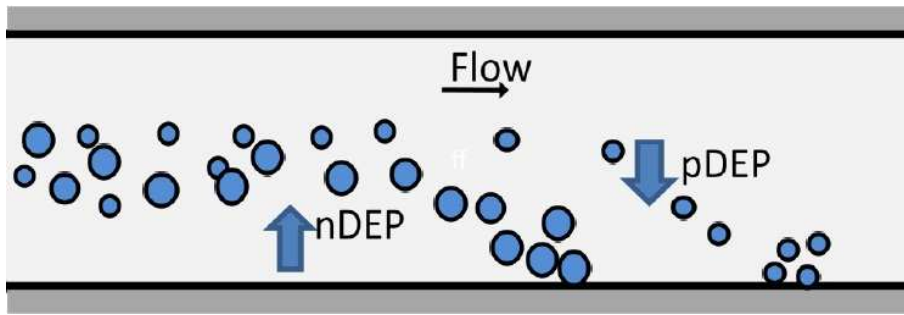


Figure 2.5: A schematic representation to show the effects of negative- and positive-dielectrophoresis in a flow field (Lin07).

Electro V6.0 software (Ies85) which combines the advantages of both the boundary element and finite element methods field solvers. It places an appropriate mesh on the model and gives confidence that it converges to stable results by basing the results on results from other meshes. In the section below a momentum transport equation is developed using both the dielectrophoretic force and the helium flow velocity profile.

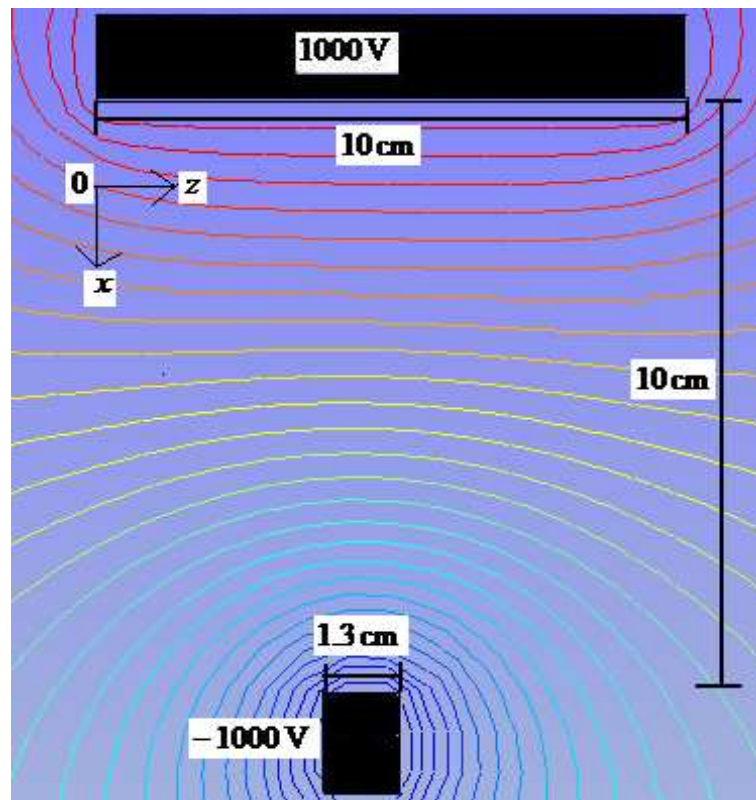


Figure 2.6: Equipotential field lines surrounding the nonuniform electrode structure made of a pin and plate configuration. The applied voltage at each electrode is $V = 1000$ volts

2.3.2 Momentum Transport Equation

Various electrohydrodynamic (EHD) forces such as Coulomb and dielectrophoretic force, convection and Brownian motion (Ram98 and Cas03) act on a particle in a fluid. However, viscous drag by the fluid (Stokes' drag for slow particles) is generally considered to have the main effect on the particle movement (Min09). In the momentum transport equation the drag force, gravity, electrostatic, centrifugal, electrophoretic and dielectrophoretic forces, as well as, the magnus force can be considered. In general spherical particles have

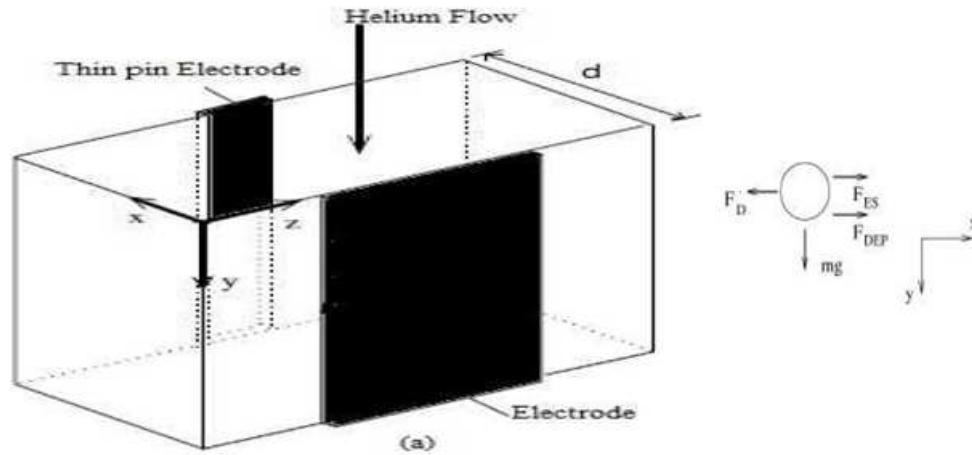


Figure 2.7: The schematic representation (a) the coordinate system and, (b) the free body force diagram.

two types of motion: translational and rotational motion. However, in this work the rotational motion is ignored (by assuming the spherical particle is very small such that the rotational effects can be ignored) and only the sum of the dielectrophoresis, electrophoresis, gravity and drag forces as the applied forces are considered. The total applied forces, $\mathbf{F}_{applied}$ of the free body diagram shown in figure 2.7 is given as (Min09)

$$\mathbf{F}_{applied} = \mathbf{F}_g + \mathbf{F}_{DEP} + \mathbf{F}_{ES} - \mathbf{F}_D, \quad (2.42)$$

where \mathbf{F}_g is the gravitational force, \mathbf{F}_{DEP} is the dielectrophoresis force, \mathbf{F}_{ES} is the electrostatic or Coulombic force and \mathbf{F}_D is the drag force. The Coulombic force is expressed as in section 2.2.4, eq. (2.31).

The drag force to be used in the calculations is determined from the value of the Reynolds number given by,

$$Re = \frac{\rho_{He} v_{ave} D_c}{\mu_{He}}. \quad (2.43)$$

where ρ_{He} is the helium density, v_{ave} is the average velocity determined from the mass flow rate when the flow profile is considered to be flat, and D_c is the characteristic diameter. When the Re of the particle is less than 0.5, the Stokes law for the drag force on a particle traveling through a fluid/medium experiences a force against the velocity as (Hua91)

$$\mathbf{F}_D = -6\pi\mu R\mathbf{v}_{rel}, \quad (2.44)$$

where, $\mathbf{v}_{rel} = \mathbf{v}_{Ag} - \mathbf{v}_{He}$, is the silver particles velocity relative to the heliums velocity and R is the particle's radius. The helium velocity is obtained from the velocity profile derived in appendix A.1.1 and given as follows,

$$v_{He} = v_{ave} \left(1 - \left(\frac{r}{R} \right)^2 \right). \quad (2.45)$$

The average velocity v_{ave} can be obtained from the mass flow rate given by,

$$\dot{m} = \rho_{He} v_{ave} A, \quad (2.46)$$

and rearranged to give,

$$v_{ave} = \frac{\dot{m}}{\rho_{He} A}. \quad (2.47)$$

where the cross-sectional area of the pipe is given as $A = \frac{\pi d^2}{4}$ and d is the diameter of the pipe. The average velocity v_{ave} in eq. (2.47) is used to calculate the Reynolds number in eq. (2.43). The density of helium ρ_{He} is derived from the ideal gas equation as follows,

$$PV = mRT, \quad (2.48)$$

$$P \frac{V}{m} = RT, \quad (2.49)$$

Therefore,

$$\frac{P}{\rho_{He}} = \left(\frac{R_u}{M_{He}} \right) T, \quad (2.50)$$

$$\rho_{He} = \left(\frac{TR_u}{PM_{He}} \right), \quad (2.51)$$

and

$$\rho_{He} = \frac{TR_g}{P}, \quad (2.52)$$

$$R_g = \frac{R_u}{M_{He}}. \quad (2.53)$$

where V is the volume (m^3), P is the pressure (MPa), T is the temperature (K), R_g is the gravitational gas constant 8.31446 J/molK and m_{He} is the mass of helium. The universal gas constant R_u is 8314.47 Nm/kmolK and the molar mass of helium M_{He} is 4 g/mol . The density of helium ρ_{He} was calculated as $\frac{(4 \times 9 \times 10^6)}{(8314.47 \times 1023)} = 4.232 \text{ kg/m}^3$. When the Knudsen number $\frac{\lambda}{2L}$ (λ is the particle mean free path and L is representative physical length scale) tends to zero, the helium in which the particle is immersed is no longer continuous and must be treated as consisting of discrete particles. Due to this phenomenon Stokes law needs to be corrected by the Cunningham correction factor C_c (Par03) as

$$F_D = \frac{6\pi\mu_{He}Rv_{rel}}{C_c}. \quad (2.54)$$

where R is the particle's radius and the viscosity μ_{He} of helium is obtained from standard tables and the value is $20.1 \times 10^{-6} \text{ kg/ms}$ at a temperature of 300 K and 1 atmospheres (Mil99). The empirical equation that provides an extension of the Stokes' law to particle range of below $0.01 \text{ }\mu\text{m}$ and less than the upper limit of $10 \text{ }\mu\text{m}$ in diameter is written as (Hin99),

$$C_c = 1 + \frac{\lambda}{d} \left[2.514 + 0.800 \times \exp\left(-0.55 \frac{\lambda}{d}\right) \right]. \quad (2.55)$$

where λ the mean free path of the gas, and d is the diameter of the particle. The acceleration of the particle can be determined from Newton's second law as

$$m_{Ag} \frac{d\mathbf{v}_{Ag}}{dt} = \mathbf{F}_g + \mathbf{F}_{DEP} + \mathbf{F}_{ES} - \mathbf{F}_D, \quad (2.56)$$

where m_{Ag} is the mass of the silver particle. Very small particles reach terminal velocity quickly. When the characteristic time scale $\frac{m_p}{6\pi\mu R}$, is about an order of magnitude smaller than the time of the numerical calculations, the assumption that very small particles reach terminal velocity quickly is no longer valid (Kan06). Appendix A.1.2 provides a detailed investigation of the terminal velocity of micro- and nanoparticles. When the particle reaches terminal velocity, the acceleration becomes negligible because the drag force is equal to the external applied forces and eq. (2.56) can be written in component form (Min09) as

$$v_x = \frac{(F_{DEP,x} + F_{ES,x})}{6\pi\mu RC_c}, \quad (2.57)$$

$$v_z = \frac{F_{DEP,z}}{6\pi\mu RC_c}, \quad (2.58)$$

$$v_y = v_{He} + \frac{(m_p g)}{6\pi\mu r}, \quad (2.59)$$

where v_x and v_z are the components of the position of the particle in the electric field plane, and v_y is the component of the particle velocity in the direction of flow. Also, $\mathbf{F}_{ES,x}$ is the Coulombic force in the x direction, while $\mathbf{F}_{DEP,x}$ and $\mathbf{F}_{DEP,z}$ are the dielectrophoretic forces in the x - and z -directions, respectively. The velocity of helium v_{He} is calculated from equation 2.45. The position, $\mathbf{p}^i(x,y,z)$, of the particle at time step i is given as

$$\mathbf{p}^i(x, y, z) = \mathbf{p}^{i-1}(x, y, z) + \mathbf{v}^{i-1}\Delta t, \quad (2.60)$$

where Δt is the time step and $\mathbf{p}^i(x,y,z)$ is the vector position of the particle at the next time step, $\mathbf{p}^{i-1}(x,y,z)$ is the vector position of the particle at the previous time step and \mathbf{v}^{i-1} is the vector velocity of the particle at the previous time step. The next chapter uses the theoretical constructed models to provide numerical simulations and discusses the numerical methods followed, as well as, the assumptions made in the numerical calculations.

Chapter 3

Numerical Simulations

The theoretical deflection models, namely the stochastic and deterministic deflection models, developed in Chapter 2 are used to calculate and predict silver particle deflections in helium using numerical algorithms. This chapter develops the numerical algorithms using the stochastic and deterministic deflection models. The chapter discusses the numerical methods, the assumptions made, and provides sample calculations from the models.

3.1 Stochastic Deflection Model

3.1.1 Numerical Method

The motion of a charged silver ion under specified starting conditions is simulated in a helium gas and under the influence of the uniform electric field. The particle assumes a random velocity within the helium gas in the system. The motion of the particle between collisions with helium atoms is subjected to a uniform electric field. The mean free time τ , of the particle between collisions is calculated in helium gas for specified pressure and temperature and is a constant value during the simulations. The magnitude of the velocity of the helium atom is randomly sampled from the velocity distribution at the specified temperature and pressure. Also, the angle that determines the direction of the particle after collision is obtain as a random

number. The time step that the particle undergoes continues until the specified elapsed time defined and restricted by the characteristic time discussed in appendix A.1.2 is complete.

3.1.2 Assumptions

The stochastic model uses Monte Carlo simulations. The elastic random collisions of a nanorange silver ion and helium atoms in the simulations are two dimensional because the electric field is a two dimensional quantity. The assumptions made are as follows:

- Collisions between the silver ion and helium atoms.
- No polyatomic and/or chemical reaction occurs (helium is inert).
- The helium gas properties such as the dielectric constant and conductivity are uniform throughout the domain.
- The particle does not alter the applied uniform electric field.
- Electric field is vertical everywhere and perpendicular to streamlines.
- The silver and helium particles are spherical and undergo elastic collisions.
- The speed of helium atoms is randomly sampled using Maxwell velocity distribution.
- Mean free time of the silver ion before the next collision is a constant.
- The angles that determines the direction of the collision are randomly sampled.

The section that follows provides sample calculations for the stochastic deflection model to illustrate the method followed in the simulations to deflect silver.

3.1.3 Sample Calculations

The sample calculations of the stochastic deflection model are done using equations that were developed in chapter 2. The applied uniform electric field strength is 100 kV/m and the silver particle is assumed to be

one ion. After 500 time steps i the silver particles x^i and z^i positions are 32.745124 mm and -0.574319 mm. The velocity of the particle in the x and z -directions ($v_{Ag,x}^i$ and $v_{Ag,z}^i$) are 319.7555654 and -116.12478 ms^{-1} , respectively. The random velocity v_{He} is obtained by choosing a random number (e.g. a value between zero and the maximum value of the cumulative distribution) and extracting its equivalent value which is then assigned as the random velocity of the helium gas. When a random number of 0.000501 is chosen the equivalent random velocity equals 1710.92 ms^{-1} . The incidence angle of the particle is randomly taken as 4.2583 rad. The x - and z -components of the relative velocity of the incident helium \mathbf{u}_{He} , were calculated as

$$\begin{aligned}
 u_{He,x} &= v_{He} \cos(\psi) - v_{Ag,x}, & (3.1) \\
 &= 1710.92 \times \cos(4.2583) - 319.755654, \\
 &= -1070.7 \text{ ms}^{-1}. \\
 u_{He,z} &= v_{He} \sin(\psi) - v_{Ag,z}, \\
 &= 1710.92 \times \sin(4.2583) + 116.12478, \\
 &= -634.821 \text{ ms}^{-1}.
 \end{aligned}$$

The magnitude of \mathbf{u}_{He} is 1244.747 ms^{-1} . The quantity arctan2 in eq. (2.27) aims to produce a value of φ such that $\pi < \varphi < \pi$, and guarantees no loss of information of the physical system when dividing two negative velocities as

$$\begin{aligned}
 \varphi &= \text{arctan2}(u_{He,z}, u_{He,x}), & (3.2) \\
 &= \text{arctan2}(-634.821, -1070.7), \\
 &= -2.60641 \text{ rad}.
 \end{aligned}$$

The collision radius divided by the radius of the silver particle, $\frac{r}{c}$, was randomly selected as -0.3015. Then, α was calculated as follows

$$\begin{aligned}\alpha &= \sin\left(\frac{r}{c}\right), \\ &= \sin(-0.3015), \\ &= -0.2965 \text{ rad.}\end{aligned}\tag{3.3}$$

Momentum is transferred only in one direction. Therefore, the velocity of helium acting in this new coordinate system \mathbf{u}'_{He} is taken as $\mathbf{u}_{He}\cos(\alpha)$ such that

$$\begin{aligned}\mathbf{u}'_{He} &= \mathbf{u}_{He}\cos(\alpha), \\ &= 1244.747 \times \cos(-0.2965), \\ &= 1190.432 \text{ ms}^{-1}.\end{aligned}\tag{3.4}$$

The velocity gained after collision due to the momentum transferred between the colliding particles is calculated as

$$\begin{aligned}\mathbf{U}'_{Ag} &= \frac{2m_{He}}{m_{He} + m_{Ag}}\mathbf{u}'_{He}, \\ &= \frac{2 \times 4}{4 + 107} \times 1244.747, \\ &= 85.79693 \text{ ms}^{-1}.\end{aligned}\tag{3.5}$$

It is necessary to transform the results back to the original coordinate system. This is done by calculating ω as

$$\begin{aligned}\omega &= \varphi - \alpha, \\ &= -2.60641 + 0.2965, \\ &= -2.30991 \text{ rad.}\end{aligned}\tag{3.6}$$

Therefore, the relative velocity of silver, U_{Ag} can be calculated in its component form as

$$\begin{aligned}
 U_{Ag,x} &= \mathbf{U}'_{Ag} \cos(\phi), & (3.7) \\
 &= 85.79693 \times \cos(-2.30991), \\
 &= -63.409585 \text{ ms}^{-1}. \\
 U_{Ag,z} &= \mathbf{U}'_{Ag} \sin(\phi), \\
 &= 85.79693 \times \sin(-2.30991), \\
 &= -57.79565 \text{ ms}^{-1}.
 \end{aligned}$$

The velocity of silver after collision is then calculated as

$$\begin{aligned}
 v_{Ag,x}^{i+1} &= v_{Ag,x}^i + U_{Ag,x}, & (3.8) \\
 &= 319.755654 - 63.409585, \\
 &= 256.346069 \text{ ms}^{-1}. \\
 v_{Ag,z}^{i+1} &= v_{Ag,z}^i + U_{Ag,z}, \\
 &= -116.12478 - 57.79565, \\
 &= -173.92043 \text{ ms}^{-1}.
 \end{aligned}$$

During the movement of silver between collisions it gains velocity in the direction of the applied electric field force (e.g. x -direction) but remains constant in the z -directions. The total velocity of the particle is then

calculated as

$$\begin{aligned}
 v_{Ag,x}^{gained} &= v_{Ag,x}^{i+1} + \frac{eE}{m_{Ag}} dt, & (3.9) \\
 &= 256.346069 + 1.6021 \times 10^{-19} \times 100000 \left(\frac{0.189285 \times 10^{-9}}{107 \times 1.66054 \times 10^{-27}} \right), \\
 &= 273.4136786 \text{ ms}^{-1}. \\
 v_{Ag,z}^{gained} &= v_{Ag,z}^{i+1}, \\
 &= -173.92043 \text{ ms}^{-1}.
 \end{aligned}$$

It follows then that the next position of the particle is calculated using the velocities in the x - and z -directions as

$$\begin{aligned}
 x^{i+1} &= x^i + v_{Ag,x}^{gained} dt, & (3.10) \\
 &= 23.745124 \times 10^{-3} + 273.4136786 \times 0.189285 \times 10^{-9}, \\
 &= 23.74517575 \text{ mm}. \\
 z^{i+1} &= z^i + v_{Ag,z}^{gained} dt, \\
 &= -0.574319 \times 10^{-3} - 173.92043 \times 0.189285 \times 10^{-9}, \\
 &= -0.57435 \text{ mm}.
 \end{aligned}$$

It is observed from the results of the sample calculations in the stochastic deflection model that the particle experiences a force that opposes its current velocity. This suggests that there exists a drag force created by the colliding of helium atoms. Therefore, the assumption made in the construction of the stochastic deflection model that the hydrodynamic drag force is incorporated within the random velocities of the helium atom is valid.

3.2 Deterministic Deflection Model

The deterministic deflection model that was developed in chapter 2 investigates the deflection of silver using a technique known as dielectrophoresis. The model studies the effects of an externally applied nonuniform electric field on a silver particle moving in a helium medium. Herein, this involves selecting a particle and studying its trajectory as it is deflected by the applied force, while ignoring its interactions with other particles within the bulk of the system, under gravity and viscous effects. The following section provides the numerical method and the assumptions made in the deterministic calculations.

3.2.1 Numerical Method

The simulations are performed within a plane of the applied electric field. The particle experiences a drag force in the helium medium. The geometrical setup is a two dimensional parallel (but unequal) electrodes placed on the surface of the helium volume. The solution to the momentum transport equation is obtained in the region of the applied electric field. Figure 3.1 shows a schematic representation of a laminar flow velocity profile. In this system (figure 3.1), the two particles are elevated against gravity to different heights because the dielectrophoretic force depends on the particle size (Lin07). Depending on the time it takes

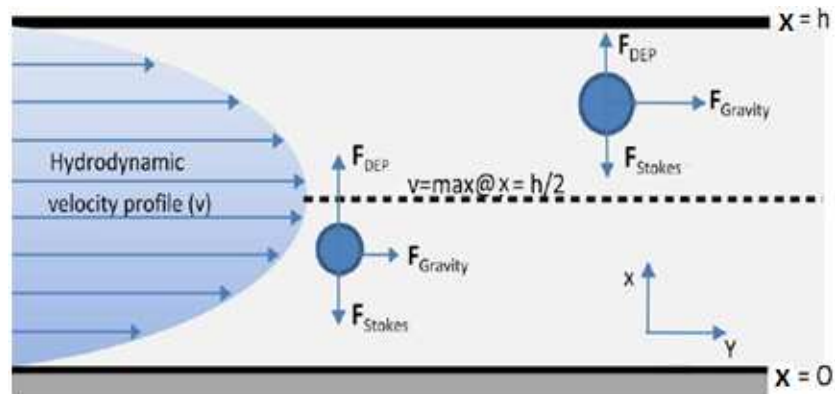


Figure 3.1: A schematic representation of a velocity profile showing the forces acting on two particles (Lin07).

to reach terminal velocity as compared to the time step either eq. (2.56) is used or the incremental eqs. (2.43), (2.44) and (2.59) are used. In the deterministic deflection model, the important properties required in the dielectrophoretic force from silver and helium are their permittivity and thermal conductivity values.

Helium as a medium has a dielectric constant, ϵ , of 1.0007 (Ata30), and the thermal conductivity, σ_{He} , is $0.152 \text{ Wm}^{-1}\text{K}^{-1}$. On the other hand, silver has a thermal conductivity, σ_{Ag} , of $429 \text{ Wm}^{-1}\text{K}^{-1}$. The Clausius Mossotti factor, K_{CM} can be calculated as a combination of the helium medium and a silver particle using eq. (2.41). The theoretically calculated values for K_{CM} is 1, $\sigma_{He} \ll \sigma_{Ag}$.

In the numerical method the dielectrophoretic force is obtained from the nonuniform electric field shown in Figure 4.4 and is a two dimensional quantity in the x - and z -directions. In the y direction, which is the direction of flow, it is assumed that the plates are long enough that the field is constant. The gravitational force calculated acts in the direction of flow together with the drag force in that direction which uses the relative velocity, \mathbf{v}_{rel} , and taking into account the helium velocity from eq. (A.12). The drag force in the direction of the electric field depends only on the velocity of the particle and the helium flow velocity is zero. The dielectrophoretic, gravitational and drag forces are included in eq. (2.56) to calculate the velocity of the particle and its position at the next step size i . The time step Δt is assumed to be $10 \mu\text{s}$. This value is used because it is less than the characteristic time of 3.16281 ms for a silver particle with a radius of $3 \mu\text{m}$ used in the simulation. However, it does not effect the time necessary to calculate the deflection path. Eq. (2.56) is used because the time step is less than the characteristic time, t_t .

3.2.2 Assumptions

The calculations obtained in the simulations follow a macroscopic theoretical deflection model developed to investigate particle deflections in a helium medium. The deflecting techniques used are dielectrophoresis and electrophoresis with consideration of the Stokes drag and gravitational force effects. The following are the assumptions made in the calculations:

- Particles are spherical in shape.
- Medium properties are uniform throughout the domain of the system.
- Particle does not alter the nonuniform electric field or the helium flow.

¹Thermal conductivity for selected materials at $\sim 300 \text{ K}$ (physics.info/conduction)

²Thermal conductivity for selected materials at $\sim 300 \text{ K}$ (physics.info/conduction)

- Rotation of the particle does not affect the particle's translational motion.
- Nonuniform electric field is two dimensional in x - and z -directions.
- Time step Δt moving the particle to the next position is $10 \mu s$.
- Reynolds number is less than 0.5 and the solution is obtained in the Stokes' region.
- The bulk velocity of the helium flow is 0.021 ms^{-1} and is used in laminar flow.
- Single out particle and deflect it by using nonuniform electric field in the helium medium.

As in the stochastic deflection model the following section provides sample calculations for the deterministic deflection model to illustrate the method followed in the numerical predictions and demonstrate the effects of nonuniform electric field in deflecting a silver microparticle.

3.2.3 Sample Calculations

This section contains a sample calculations of the deterministic deflection model. The model is used together with the numerical simulations to predict the deflection of a silver particle with a radius of $3 \mu m$ in a nonhomogeneous electric field. The forces that are considered to be acting on the particle in this calculations are the dielectrophoretic force, drag force and gravitational force. The x - and z -components of the dielectrophoretic force are calculated using the nonuniform electric field shown in Figure 4.4 as follows

$$\begin{aligned}
 F_{DEP,x} &= 2\pi\epsilon_{He}K_{CM}r^3\nabla E_x^2 & (3.11) \\
 &= 4\pi(1.00007 \times 8.85418 \times 10^{-12}F/m)(3 \times 10^{-6}m)^3 \times (-3963.96) \\
 &= -1.19092 \times 10^{-23} \text{ N}. \\
 F_{DEP,z} &= 2\pi\epsilon_{He}K_{CM}r^3\nabla E_z^2 \\
 &= 4\pi(1.00007 \times 8.85418 \times 10^{-12}F/m)(3 \times 10^{-6}m)^3 \times (-381101.10) \\
 &= -1.14497 \times 10^{-24} \text{ N}.
 \end{aligned}$$

The magnitude of the gravitational force in the direction of flow can be calculated as

$$\begin{aligned}
 F_{g,y} &= mg = \rho_{Ag} \times \frac{3}{4}\pi R^3 \times g \\
 &= 10500 \text{kgm}^{-3} \times \frac{4}{3}\pi (3 \times 10^{-6} \text{m})^3 \times 9.81 \text{ms}^{-2} \\
 &= 1.16496 \times 10^{-11} \text{ N}.
 \end{aligned} \tag{3.12}$$

The mean free path, λ , is a necessary quantity in order to calculate the correction factor, C_c , for the drag force λ is calculated as (Ste09)

$$\begin{aligned}
 \lambda &= \frac{RT}{\sqrt{2}\pi d^2 N_{Ap}} \\
 &= \frac{k_B T}{\sqrt{2}\pi d^2 p} \\
 &= \frac{1.3806504 \times 10^{-23} \text{J/K} \times 293.15 \text{K}}{\sqrt{2}\pi \times (0.098 \times 10^{-9} \text{m})^2 \times 98066.5 \text{Pa}} \\
 &= 966.78 \times 10^{-9} \text{ m}.
 \end{aligned} \tag{3.13}$$

The mean free path calculated in eq. (3.13) is used together with the diameter of the particle to determine the Cunningham correction factor, C_c , as

$$\begin{aligned}
 C_c &= 1 + \frac{\lambda}{d} \left[2.514 + 0.800 \times \exp\left(-0.55 \frac{\lambda}{d}\right) \right], \\
 &= 1 + \frac{241.8109 \times 10^{-9}}{2 \times 3 \times 10^{-6}} \left[2.514 + 0.800 \times \exp\left(-0.55 \frac{241.8109 \times 10^{-9}}{2 \times 3 \times 10^{-6}}\right) \right], \\
 &= 1.132853.
 \end{aligned} \tag{3.14}$$

The velocity of the helium medium at a specified *position*, 0.56453 nm, can be calculated using the helium velocity profile eq. (A.12) as

$$\begin{aligned}
 v_{He} &= v_{max} \left(1 - \left(\frac{\text{Position}}{h} \right)^2 \right) \\
 &= 0.021 \text{ms}^{-1} \times \left(1 - \left(\frac{0.56453 \times 10^{-9} \text{m}}{(10 \times 10^{-2}) \text{m}} \right)^2 \right) \\
 &= 0.021 \text{ ms}^{-1}.
 \end{aligned} \tag{3.15}$$

where h is the height of the pipe. The particles deflection distance can be calculated using the dielectrophoretic force, the gravitational force and the drag force by taking into account the helium flow and assuming that the particles are not charged. The time it takes a particle of $3 \mu\text{m}$ radius to reach terminal velocity is $3162.81 \mu\text{s}$ (see Table A.1). This value is larger than the time step, dt , of $10 \mu\text{s}$ which was assumed for the calculations. Therefore, the incremental eqs. (2.43), (2.44) and (2.45) are no longer valid because the particle has not reached terminal velocity. It is now necessary to employ Newton's second law eq. (2.56) to predict the deflections. Consider a particle that has travelled approximately $50 \mu\text{s}$ in the system, its velocity components are, $v_x^i = -1.13182 \times 10^{-05} \text{ ms}^{-1}$, $v_y^i = 3.369 \times 10^{-3} \text{ ms}^{-1}$ and $v_z^i = -6.21216 \times 10^{-07} \text{ ms}^{-1}$. Rearranging eq. (2.56) and extracting explicitly the x -component of the velocity gives

$$\begin{aligned}
v_x^{i+1} &= v_x^i + \left(F_{DEP,x} - \frac{F_{D,x}}{C_c} \right) \frac{dt}{m_{Ag}} & (3.16) \\
&= -1.13182 \times 10^{-05} + \frac{10 \times 10^{-6}}{10500 \times \frac{4}{3} \times \pi \times (3 \times 10^{-6})^3} \\
&\times \left(-1.19092 \times 10^{-23} + \frac{1.13182 \times 10^{-05} \times 6 \times \pi \times 3 \times 10^{-6} \times 20.1 \times 10^{-6}}{1.132853} \right) \\
&= -1.12226 \times 10^{-5} \text{ ms}^{-1}.
\end{aligned}$$

The y -component of the velocity is

$$\begin{aligned}
v_y^{i+1} &= v_y^i + \left(F_{g,y} - \frac{F_{D,y}}{C_c} \right) \frac{dt}{m_{Ag}} & (3.17) \\
&= 19.4901 \times 10^{-3} + \frac{10 \times 10^{-6}}{10500 \times \frac{4}{3} \times \pi \times (3 \times 10^{-6})^3} \\
&\times \left(1.16496 \times 10^{-11} - \frac{(3.369 - 21.0) \times 10^{-3} \times 6 \times \pi \times 3 \times 20.1 \times 10^{-12}}{1.132853} \right) \\
&= 3.616064 \times 10^{-3} \text{ ms}^{-1}.
\end{aligned}$$

The calculation of the particle speed in the z -direction is given as

$$\begin{aligned}
v_z^{i+1} &= v_z^i + \left(F_{DEP,z} - \frac{F_{D,z}}{C_c} \right) \frac{dt}{m_{Ag}} & (3.18) \\
&= -6.21216 \times 10^{-07} + \frac{10 \times 10^{-6}}{10500 \times \frac{4}{3} \times \pi \times (3 \times 10^{-6})^3} \\
&\times \left(-1.14497 \times 10^{-24} - \frac{6.21216 \times 10^{-07} \times 6 \times \pi \times 3 \times 20.1 \times 10^{-12}}{1.132853} \right) \\
&= -6.15967 \times 10^{-7} \text{ m s}^{-1}.
\end{aligned}$$

The particles current position, after $50.999 \mu\text{s}$, is ($x^i = 0.56453 \text{ nm}$, $y^i = 128.56724 \text{ nm}$, $z^i = 0.99426 \text{ nm}$).

Then eq. (2.60) can be used for the x -, y -, and z -components to obtain the next position. In the x -direction the position is

$$\begin{aligned}
x^{i+1} &= x^i + v_x^{i+1} dt & (3.19) \\
&= 0.56453 \times 10^{-9} - 1.12226 \times 10^{-5} \times 10 \times 10^{-6} \\
&= 0.452124 \times 10^{-9} \text{ m}.
\end{aligned}$$

The position calculated in the y -direction is

$$\begin{aligned}
y^{i+1} &= y^i + v_y^{i+1} dt & (3.20) \\
&= 128.56724 \times 10^{-9} + 3.616064 \times 10^{-3} \times 10 \times 10^{-6} \\
&= 124.7276 \times 10^{-9} \text{ m}.
\end{aligned}$$

Finally, in the z -direction the position is calculated as

$$\begin{aligned}
z^{i+1} &= z^i + v_z^{i+1} dt & (3.21) \\
&= 0.99426 \times 10^{-9} - 6.15967 \times 10^{-7} \times 10 \times 10^{-6} \\
&= 0.9881 \times 10^{-9} \text{ m}.
\end{aligned}$$

In the sample calculations for the deterministic deflection model using dielectrophoresis, the velocity of a silver particle is greater in the y -direction when compared to either the x or z velocities produced from the dielectrophoretic forces. This becomes evident when a comparison is made between the gravitational force and the dielectrophoretic forces and suggests that dielectrophoretic force is negligibly small at the helium bulk velocity of 0.021 ms^{-1} . A conclusion can be drawn that dielectrophoresis is not an appropriate option for deflecting particles under conditions created in this work.

Chapter 4

Results and Discussions

4.1 Stochastic Deflection Model

4.1.1 Electrophoresis

The results discussed in this chapter are obtained using the theoretical models developed in chapter 2 together with the numerical methods developed in chapter 3. In the stochastic deflection model the motion of a charged silver ion is simulated in a helium gas. The motion of the particle between collisions is subjected to the influence of a uniform electric field (electrophoresis). As the particle collides with the helium gas atoms it assumes a random velocity within the bulk of the system. The simulations are performed using an algorithm that is characterized by a flow chart shown in Figure B.1, Appendix B. The solution is governed by a number of equations that defines the physical state of the system. The Maxwell velocity distribution plays a significant role in the system because it is a statistical function that can be used to determine random velocities of helium atoms. Figure 4.1(a) shows the theoretical Maxwell velocity distribution, and the random velocity distribution obtained from binned random speeds of helium atoms. The data was obtained from the rejection method developed in a Python algorithm. The method rejects all the velocities that lie outside the Maxwell velocity distribution. Figure 4.1(b) shows the cumulative part of the helium's random

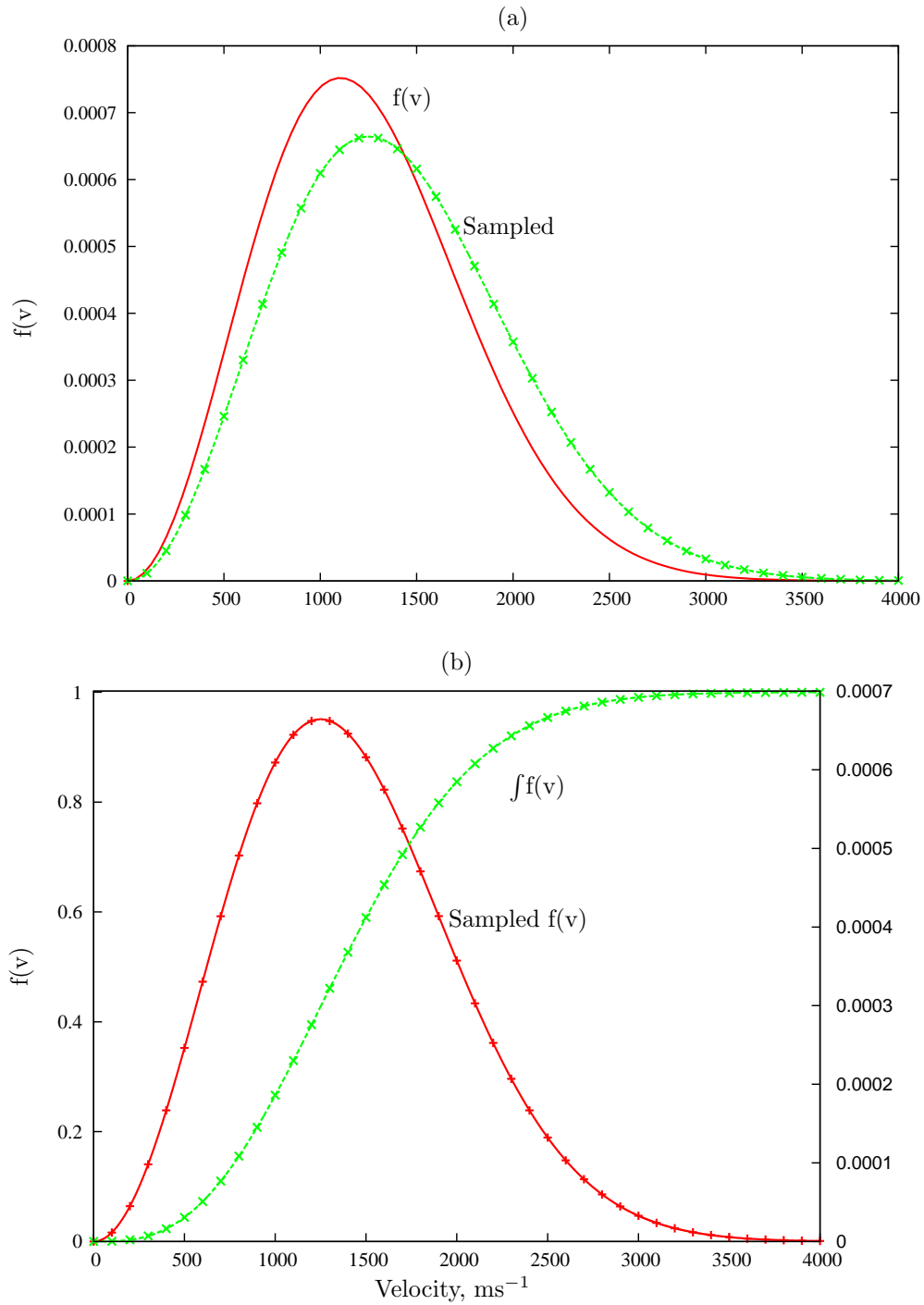


Figure 4.1: Helium velocity distributions: Figure (a) shows a comparison of the theoretical Maxwell-Boltzmann velocity distribution from eq. (2.10) normalized with respect to probable velocity (Temperature $T = 20^\circ \text{ C}$ and pressure $P = 1 \text{ atm}$), and the random velocities of helium atoms binned into a distribution. Figure (b) shows a comparison of randomly sampled helium velocity distributions, and the cumulative velocity distribution.

velocity distribution, and compares it with the helium's random velocity distribution.

In the simulation, each step taken before a collision consists of giving the helium atom a random velocity and obtaining a mean free time value, which is constant and calculated using eq. (2.13). The particle is subjected to a uniform electric field and a new position is calculated at the end of the mean free time until the simulation time is complete. Table 4.1 shows the deflection results from the stochastic simulations with pressure and temperature of 1 bar and 20 °C, respectively. The mean free time the particle spends without colliding with helium atoms is 0.189285 ns. The results show that for the simulation time of a 0.1 μ s the total deflection distances increase (16.23, 33.38 and 66.63 mm) as the applied electric field strength increases (50000, 100000, and 200000 Volts/meter), respectively. Table 4.2 shows the total deflection distances for a pressure of 90 bar, a temperature of 900 °C, a mean free time of 0.004207 ns and a simulation time of 0.1 μ s. It is observed that the total deflection distances increase (0.25, 0.88 and 1.86 mm) as the applied electric field strength increases (5000, 100000, and 200000 Volts/meter), respectively.

Table 4.1: Deflection results from the stochastic simulations with pressure and temperature of 1 bar and 20 °C, respectively. The time that the particle spends without colliding is calculated in the simulations as a constant value of 0.189285 ns.

Simulation Time μ s	Electric Field Volts/meter	Deflection mm	Execution Time s
0.1	50000	16.23	21
0.1	100000	33.38	7
0.1	200000	66.63	7
1.0	50000	159.56	13
1.0	100000	327.80	10
1.0	200000	654.25	12

Table 4.2: Deflection results from the stochastic simulations with pressure and temperature as 90 bar and 900 °C, respectively. The time that the particle spends without colliding is calculated in the simulations as a constant value of 0.004207 ns.

Simulation Time μ s	Electric Field Volts/meter	Deflection mm	Execution Time s
0.1	50000	0.25	34
0.1	100000	0.88	30
0.1	200000	1.86	35
1.0	50000	2.38	231
1.0	100000	8.73	233
1.0	200000	18.61	236

To get a good sense of the deviation in the results some of the values are compared to the work done by Cronje (2007), in which silver ions were deflected using uniform electric fields. Steyn (2009) performed the same calculations and his results are also given. Table 4.3 shows a comparison of the deflection results obtained in this work with those from Cronje and Steyn at different temperature and pressure and a pre-defined simulation time of 0.1 μ s. The expression used to determine the deviation from Cronje (2007) is given as $\frac{(Cronje-Mokgalapa) \times 100^\circ / \circ}{Cronje}$ and is shown in the last column of Table 4.3. For example, the deviation (between Cronje's work and the work done in this research) in the deflection of a silver ion as it collides with helium gas and under the influence of a uniform electric field of 100000 Volts/meter at a temperature of 20 $^\circ$ C is 13.26 $^\circ / \circ$. This may be due to the fact that in Cronje's work a random free time distribution was used to generate random free times that the particle spends before the next collision. However, in this work a constant value for the free time was used through out the simulations. Figure 4.2 shows comparison between Cronje results and the results obtained from the work done in this research. The deviation is large when the temperature is 20 $^\circ$ C and the pressure is 1 bar. The results are comparable when the temperature is 900 $^\circ$ C and the pressure is 90 bar. This suggests that temperature and pressure play a role in the physical system. Debugging was extensively performed to test and check the program for errors and making sure that the program performs as intended. However, it is possible that other errors, such as, logic computer errors (which are hard to find and fix) may have prevented the accuracy of the programs.

Table 4.3: Deflection comparison between the simulations and results from Cronje (2007) and Steyn (2009). The results are compared for different temperature and pressure and for a predefine time of 0.1 μ s.

P	T $^\circ$ C	E_{Field} V/m	Deflection, mm			$\frac{(Cronje-Mokgalapa) \times 100}{Cronje}$ $^\circ / \circ$
			Cronje	Steyn	Mokgalapa	
1 atm	20	50000	18.70	17.69	16.22	13.262
1 atm	20	100000	37.40	35.72	33.38	10.749
90 bar	900	100000	0.875	0.816	0.876	0.114
90 bar	900	200000	1.709	1.619	1.861	8.894

Cronje (2007) and Steyn (2009) validated their models by comparing the silver random velocity distribution produced from velocities of silver obtained after collisions with helium atoms with the theoretical velocity distribution for silver. They observed that the velocity distribution of silver ion follows a Maxwellian dis-

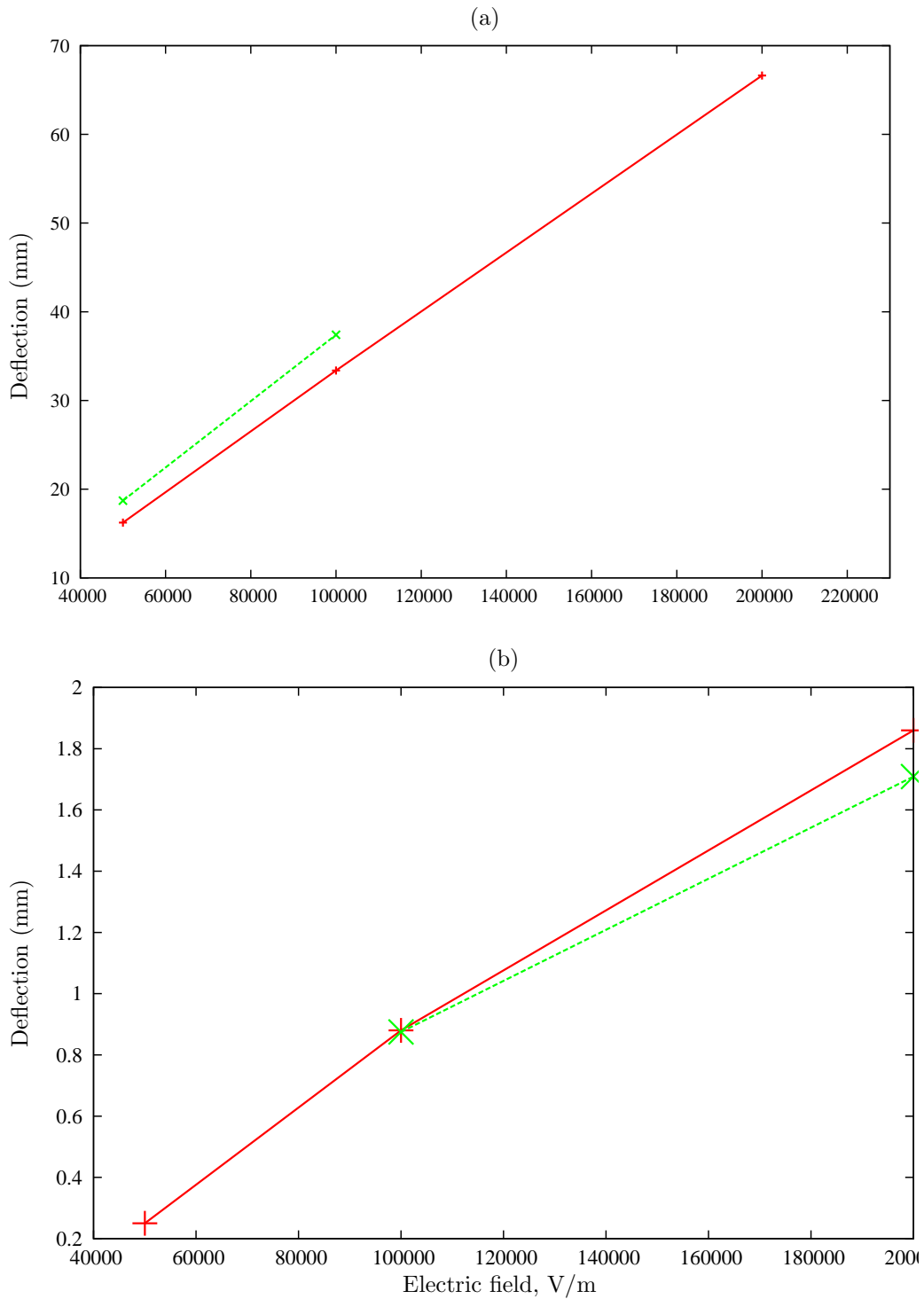


Figure 4.2: Comparison between Cronje results (broken lines) and values obtained from work done in this thesis (solid line) for the simulation time of $0.1 \mu\text{s}$: (a) the temperature is $20 \text{ }^\circ\text{C}$ and the pressure is 1 bar, (b) the temperature is $900 \text{ }^\circ\text{C}$ and the pressure is 90 bar.

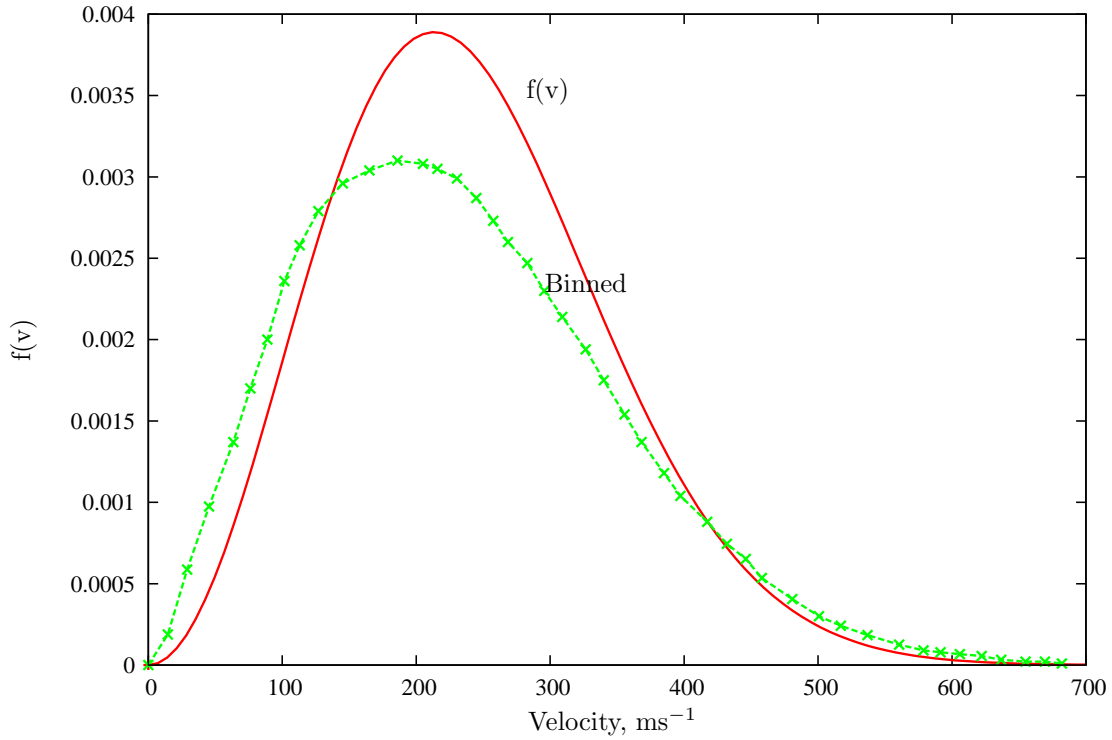


Figure 4.3: Maxwellian velocity distribution for silver particles after collisions (a) random velocity distribution, and (b) theoretical distribution from eq. (2.10) for silver at $T = 20^\circ \text{C}$ and 1 atm.

tribution (Cro07, Ste09) and concluded that the simulations they conducted obey a proper physical state. It is then necessary to verify the same concept for the simulations done in this work by accumulating and binning random velocities of a silver particle and analyzing the distribution. Figure 4.3(a) is random velocity distribution of a silver particle for after collision velocities with helium atoms. While figure 4.3(b) is theoretical distribution of silver at $T = 20^\circ \text{C}$ and 1 bar. The random and theoretical distributions in Figure 4.3 are compared on the same scale. A possible reason from the deviation of the random velocity distribution of silver ions from the theoretical Maxwell velocity distribution may be a lack of enough data, this is because there are only 45 bins in the binned random velocities and the repetition of simulations may have been too little to provide better results. However, the random velocity distribution still shows a Maxwell velocity distribution trend and provides confidence that the simulations performed in this work converged to a proper physical state expressed by a Maxwell velocity distribution. A uniform electric field used in this work is advantageous because the field force is always in the same direction and independent

of the particles's velocity, hence it is expected to be more efficient than magnetic field force as suggested by Cronje (Cro07). However, it was observed in the simulations that the mean free times are short where for 20° C and, 1 bar the free time is 0.189285 ns and for the temperature of 900° C and the pressure 90 bar the free time is 0.004207 ns. This implies that the time taken by a particle between collisions is not enough for appreciable deflections to occur.

4.1.2 Dielectrophoresis

The stochastic model can also be used to describe the deflection of a silver atom due to a dielectrophoretic force. In this case the atom would theoretically be attracted to the region of strong electric fields if it experiences positive-dielectrophoresis and the region of low electric fields if it experiences negative-dielectrophoresis. The static average electric dipole polarizability for ground state silver atoms has been theoretically calculated as $8.56 \times 10^{-24} \text{ cm}^3$ (Lid96). To obtain the force on the particle due to the polarizability of the atom in a nonhomogeneous electric field, eq. (2.34) can be used. In this work an analytical calculation of the velocity achieved by the silver atom due to Brownian motion and dielectrophoretic forces are calculated and compared to determine the viability of dielectrophoresis in the stochastic simulations. In the Brownian motion the most probable speed v_p of helium at 1 atm is calculated by means of eq. (2.7), $(2 \times 8.31436 \times 293.15)/(4/1000) = 1103.994 \text{ ms}^{-1}$. This v_p is then used as the velocity of helium, \mathbf{u}_{He} , in equation 3.5 to calculate the velocity gained by silver atoms as; $((2 \times 4)/(4 + 107)) \times 1103.994 = 79.563 \text{ ms}^{-1}$. The dielectrophoretic force due to polarizability of the atom was calculated for the same nonhomogeneous electric field in figure 4.4 at a particular point (i.e. $(2 \times \pi \times 8.56 \times 10^{-24} \text{ cm}^3 \times 8.854 \times 10^{-12} \text{ F/m} (4625.2799 \text{ V}^2/\text{m}^2))$) and gave a value of $4.40524 \times 10^{-30} \text{ N}$. Using the rearranged version of eq. (2.56), the change in velocity which the force, \mathbf{F}_α , contributes to the motion of the atom was calculated, $(4.40524 \times 10^{-30} \times 0.189285 \times 10^{-9})/(107 \times 1.66 \times 10^{-27})$, and a resulting velocity of $4.69455 \times 10^{-6} \text{ nms}^{-1}$. The two velocities are compared (i.e. 79.563 ms^{-1} vs. $4.69455 \times 10^{-6} \text{ nms}^{-1}$) and suggests that the dielectrophoretic force due to polarizability of the silver atom, is far less than the force due to momentum transfer during collisions with the helium atoms. This indicates that the particles motion is far more dependent on the effects of Brownian motion than the dielectrophoretic force making dielectrophoresis negligible in deflecting silver to the wall of a hotpipe. In

the following discussion, dielectrophoresis is explored in the deterministic deflection model to investigate its viability to deflect microparticles.

4.2 Deterministic Deflection Model

In the deterministic deflection model, the main force is the dielectrophoretic force, F_{DEP} . This force is obtained from the nonuniform electric field and acts in the x - and z -directions only. Figure 4.4 shows a nonuniform electric field distribution. The field is created by two inhomogeneous electrodes that are 10 cm apart with an applied voltage of 1000 Volts on each electrode. Each arrow represents the amplitude and

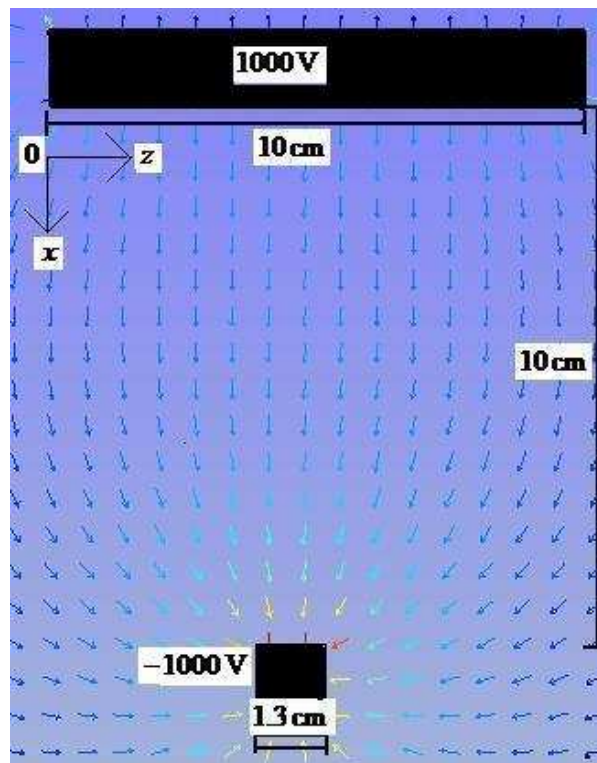


Figure 4.4: Nonuniform electric field distribution on a nonsimilar electrode structure. Each arrow represents the amplitude and direction of the electric field at the center of its tail.

direction of the electric field at the center of its tail. The nonuniform electric field was generated in the x - and z -directions by assuming that in the y -direction, which is the direction of flow, the electrodes are long enough such that the field is constant in that direction. The gravitational force and the drag force are calculated in the direction of flow, and the drag force in that direction incorporates the helium velocity

through the relative velocity, v_{rel} , of the particle given in equation 2.44. In order to determine whether eq. 2.56 or the incremental eq 2.43, 2.44 and 2.59 are to be used, it is necessary to determine whether the deflected particle reaches terminal velocity or is continuously accelerated. Table A.1 in appendix A shows values of the time at which the particle of a specific size reaches terminal velocity. The particle used in this work has a radius of $3 \mu\text{m}$, and so the time it would take the particle to reach its terminal velocity is 3.16281 ms. This value is larger than the time step of $10 \mu\text{s}$. Therefore, eq. 2.56 was used to determine the discrete velocity and position of the particle at each time step. Table 4.4 shows silver particle deflection for the deterministic deflection model in a nonuniform electric field.

Table 4.4: Particle deflection results for the deterministic deflection model with contributions from dielectrophoretic for a specific initial conditions. The single clustered silver particle with a size of $3 \mu\text{m}$. The numerical calculation time is $50.999 \mu\text{s}$.

Points in Field	x nm	y nm	v_x ms^{-1}	v_z ms^{-1}
5,1	0.56453	0.99426	-1.13182×10^{-05}	-6.21216×10^{-07}
5,2	0.47266	1.99880	-1.55838×10^{-05}	$-2.612289 \times 10^{-07}$
5,3	0.40548	3.00023	-1.98061×10^{-05}	-5.12055×10^{-08}
5,4	0.39603	4.00015	-2.08207×10^{-05}	-2.20015×10^{-08}
5,5	0.44519	4.99952	-1.72225×10^{-05}	-1.11728×10^{-07}
5,6	0.52898	5.99944	-1.28013×10^{-05}	-1.20856×10^{-07}
5,7	0.62417	6.99958	-9.18931×10^{-06}	-7.90260×10^{-08}
5,8	0.72609	7.99856	-6.36130×10^{-06}	-5.79908×10^{-08}

The results on total deflection distance in table 4.4 shown that the dielectrophoretic force is not an appropriate method in deflecting particles, especially when the particle spends a short time (e.g. $50.999 \mu\text{s}$) in the electric field. Figure 4.5(a) shows the trajectory of a silver particle radius $3 \mu\text{m}$ deflected in a nonuniform electric field. The deflection starts at a randomly sampled position in the electric field, (i.e. 0 nm in the z - and 1 nm in the x -direction of the position). The particle's initial velocity is zero in both z - and x -directions. The total deflection distance in the z - and x -components of the position are -33.4 nm and 0.657 nm, respectively. The deflection results in Figure 4.5(a) are presented varying with time as shown in Figures 4.5(b) and 4.5(c). The trajectories show that as time increases the deflections also increase due to the increase in the electric field. An increase in the velocities is observed by an increase in the spacing between data points. The deflection of a silver particle is obtained at a different arbitrary location in the electric field by giving the particle an initial position (i.e. 1 nm in the x - and 8.0004 nm in the z -direction of the position) and zero

initial velocities. At the new location the results are obtained for the x - and z -components of the particle's position varying with time as shown in Figures 4.6(b) and (c). The trajectories show an increase in the particle's speed as the time increases and, the increase the speed can be observed due to the increase in the spacing between data points. The trend may be due to an increase in the electric field strength as the particle is deflected further in the electric field with time. The results show that the total deflection distance the particle travels due to a dielectrophoretic force is negligibly small and suggests that the dielectrophoresis is not an appropriate option to deflect silver particles. The time that the particle spends in the electric field was very small, $50.999 \mu\text{s}$, for the particle to experience larger deflections. It would be interesting to observe how large deflections can get when the particle travels for a longer time in the electric field. Dielectrophoresis is generally used in microchannels instead of centimeters and the deflections might be appreciable although microchannels would not be suitable to deflect silver particles in a helium hot pipe.

A comparison between the dielectrophoretic forces ($F_{DEP,x}$ of -1.19092×10^{-23} N and $F_{DEP,z}$ of -1.14497×10^{-24} N) and the gravitational force (1.16496×10^{-11} N) shows that the gravitational force is much larger and overshadows the dielectrophoretic force. The results show that dielectrophoresis is not a suitable means deflecting particles to the helium hot pipe wall to scrub them. This was shown in the stochastic deflection model by comparing dielectrophoresis to the Brownian motion, and later in the deterministic deflection model by comparing dielectrophoresis to gravitational force. Dielectrophoresis can perhaps be improved by using microchannels such as in biological applications where gravity can be ignored.

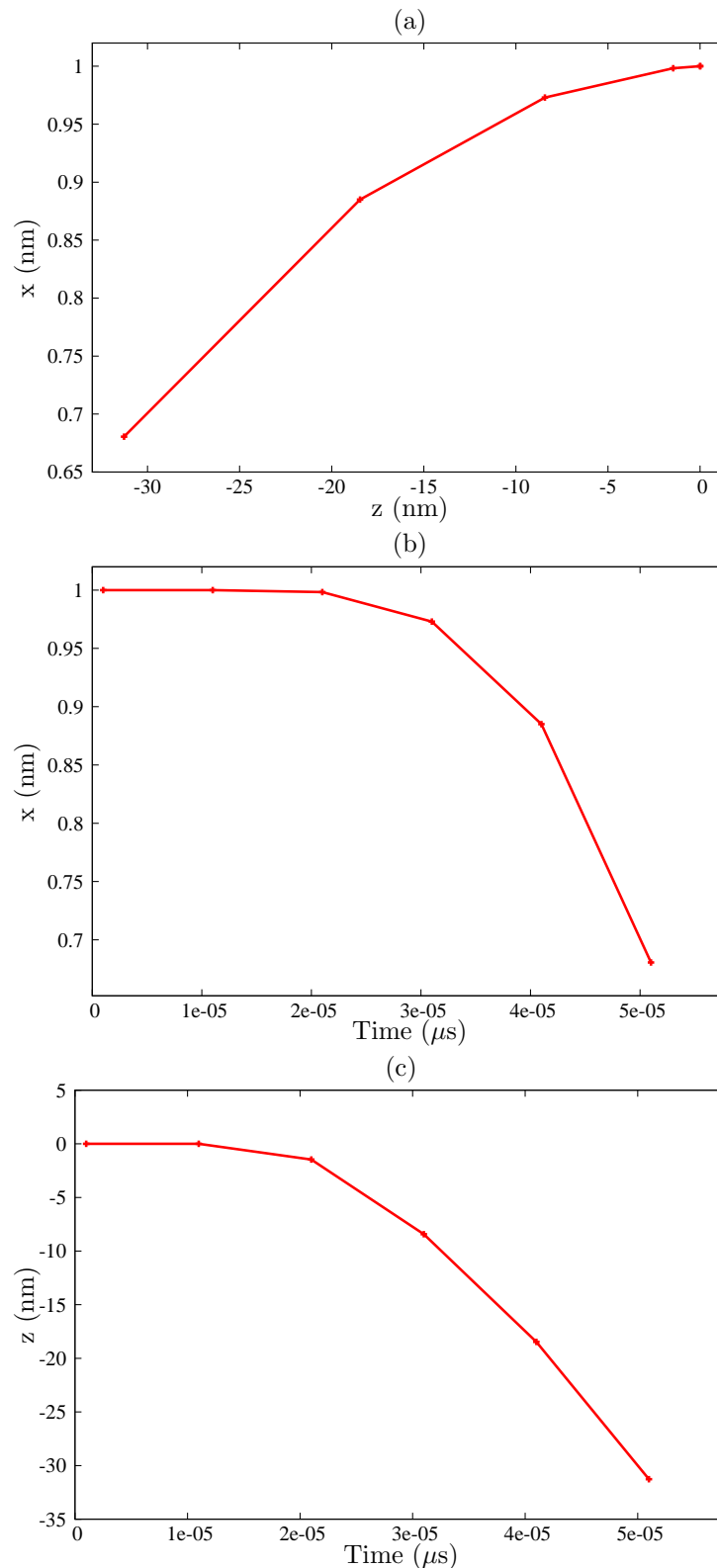


Figure 4.5: The trajectory of a silver particle (radius $3 \mu\text{m}$) deflected in a nonuniform electric field under the deterministic deflection model (using components of equation 2.60). The deflections start at an arbitrary location 1: (a) is a projection in the field plane with x - and z -components of the position; (b) is the x -component of the position varying with time; and (c) is z -components of the position varying with time. The numerical calculation time is $50.999 \mu\text{s}$. Note: x is the direction from one plate to the other and z is the direction across the plates.

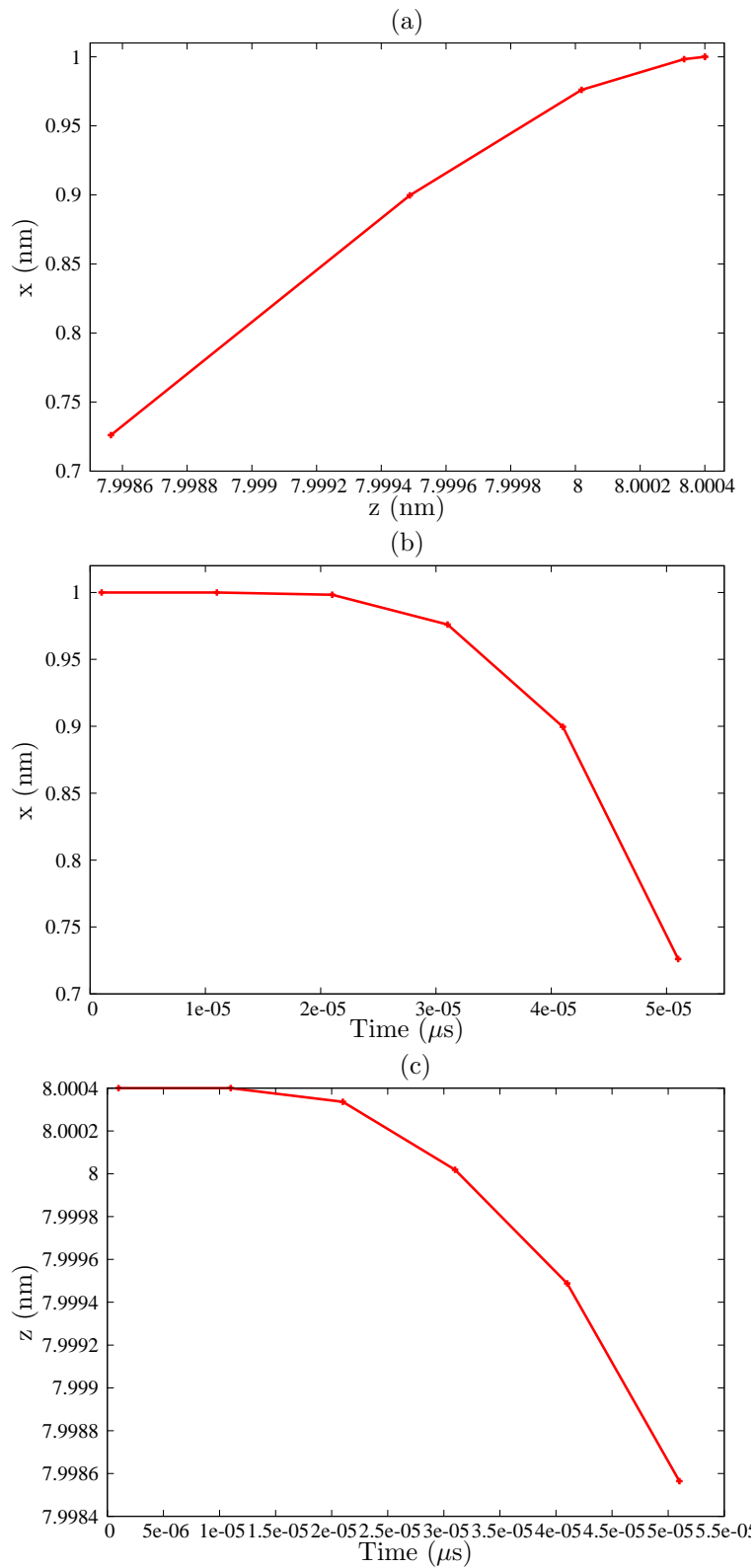


Figure 4.6: The trajectory of a silver particle (radius $3 \mu\text{m}$) deflected in a nonuniform electric field under the deterministic deflection model (using components of equation 2.60). The deflections start from at an arbitrary location 2: (a) is a projection in the field plane with x - and z -components of the position; (b) is the x -component of the position varying with time; and (c) is z -components of the position varying with time. The numerical calculation time is $50.999 \mu\text{s}$. Note: x is the direction from one plate to the other and z is the direction across the plates.

Chapter 5

Discussions and Conclusions

5.1 Stochastic Deflection Model

A stochastic deflection model was considered as an option for deflecting silver particles. In this work the model was used to investigate the viability of deflecting silver ions and/or atoms moving in a helium gas using a uniform electric field (electrophoresis) and a nonuniform electric field (dielectrophoresis). The latter uses a principle of translational motion of a neutral particle caused by polarization effects in a nonuniform electric field. In dielectrophoresis a neutral particle experiencing a positive dielectrophoretic force moves towards a region of a high electric field strength, and to a region of a low electric field strength when experiencing a negative dielectrophoresis, regardless of the electric field polarity. The former method follows the principal that opposite charges attract and similar charges repel and requires the particle to be charged.

5.1.1 Electrophoresis

In the stochastic deflection model the motion of a silver particle was simulated as the particle collided with helium atoms in the bulk of the system. After each collision the particle was given a mean free time and was subjected to a uniform electric field (e.g. electrophoresis) until the next collision. In the simulations the helium atoms were given random velocities (extracted from the Maxwell velocity distribution) prior to

colliding with a silver particle. As the particle collides with the helium atoms it assumed random velocities, imparted to it by the helium atoms, within the bulk of the system. The random velocities of the silver particles after collision with helium atoms were binned into a distribution and then compared to the theoretical Maxwell velocity distribution for silver at 20 °C and 1 bar. When these distributions were compared on the same scale (see figure 4.3 chapter 4), they did not fit but the random velocity distribution of silver follows Maxwell velocity distribution. This trend was in line with what Cronje (2007) and Steyn (2009) determined in their results. In conclusion, the simulations performed in this work converged to a proper physical state expressed by a Maxwell velocity distribution and gave confidence in the results discussed.

In the simulations, a silver particle was deflected at a temperature of 20 °C and 900 °C, and a pressure of 1 bar and 90 bar, respectively. Each simulation was allowed to run for a simulation time of 0.1 μ s and repeated for statistical accuracy. The total deflection values that were obtained are 16.22 mm and 33.38 mm for a temperature of 20 °C and a pressure of 1 bar with applied electric field strengths of 50000 and 100000 V/m, respectively. At a temperature of 900 °C and 90 bar the total deflection values were 0.876 mm and 1.861 mm for applied electric field strengths of 100000 and 200000 V/m, respectively. The total deflection values were then compared to Cronje's (2007) results (e.g. 18.70 mm, 37.4 mm, 0.875 mm and 1.709 mm) and Steyn's (2009) results (e.g. 17.69 mm, 35.72 mm, 0.816 mm and 1.619 mm) obtained under the same temperature, pressure and electric field strengths as in this research. The results are in good agreement deviations ranging from 0.11 to 13.26 %.

The large deviations may come from the fact that in Cronje's (2007) work a random free time distribution generator was used to generate random mean free time between collisions of silver with helium atoms. In this work however, a constant value for the mean free time was used between collisions throughout the simulations. In conclusion, the deflection results suggest that the stochastic deflection model is a possible technique for the deflection of silver particles using a uniform electric field. This is due to the fact that the uniform electric field is always in the same direction and independent of the particle's velocity. However, the mean free times are short (0.189285 ns at 20 °C and 1 bar and 0.004207 ns at 900 °C and 90 bar) such that there is not enough time for a particle to be appreciably deflected by the electric field between collisions. This explains the small total deflection values obtained in this research.

Sample calculations for the stochastic deflection model were conducted to determine deflections and verify

the effects of a short mean free time. In the calculations (chapter 3, section 3.1.3) a particle was considered after a number of time steps (e.g. 500 steps). At this time step the position of the particle was 23.745124 mm in the x - and -0.574319 mm in the z -direction. After the 100 kV/m electric field was applied the particle moved to the next position at 23.745175 mm in the x -direction and -0.574350 mm in the z -direction. The change in position of the silver particle constituted a movement of 5.175 nm in the x -direction, which is the direction of the uniform electric field, and 31.0 nm in the z -direction, which was influenced by the Brownian motion alone.

In conclusion, the values obtained in the sample calculations, for the change in position of the particle, suggests that the silver particle experienced an opposing force to its current motion. This suggests that a drag force existed and was created by the collisions of silver with helium atoms. As a result, the assumption that was made in chapter 2, section 2.3.2, that the hydrodynamic drag force that is incorporated in the random velocities of the helium atom is valid.

5.1.2 Dielectrophoresis

The stochastic model was used to investigate the deflection of a silver atom due to a dielectrophoretic force. According to dielectrophoresis the atom would theoretically be attracted to the region of a strong electric field if it experiences positive-dielectrophoresis and the region of a low electric field when experiencing negative-dielectrophoresis. A dielectrophoretic force due to polarization of a silver atom in a nonuniform electric field was used in a simple calculation of the stochastic deflection model (chapter 4 section 3.2.3). The force produced from a nonuniform electric field, 4.40524×10^{-30} N, was used to calculate the speed that the particle would reach under the influence of a nonuniform electric field and gave a speed of 4.69455×10^6 nms⁻¹. The speed reached by a silver atom due to Brownian motion was also calculated as 79.563 ms⁻¹. The two results suggested that the dielectrophoretic force due to polarizability of the silver atom, is far less than the force due to momentum transfer during collisions of the silver atom with the helium atoms. In conclusion, the particles motion is far more dependent on the effects of Brownian motion than the dielectrophoretic force. This means that dielectrophoresis is not really an option to consider as an appropriate method in deflecting a

silver atom when using the stochastic deflection model. The dielectrophoresis can be used in a deterministic deflection model by exploiting the dielectric and conductivity properties of the particle and the medium, respectively.

5.2 Deterministic Deflection Model

The deterministic deflection model was also considered in investigating the deflection of particles. In this model dielectrophoresis was used as a technique to deflect neutral silver particles. The radius of the silver particle in consideration was $3\ \mu\text{m}$, and the numerical time step was $10\ \mu\text{s}$; this value was chosen because it is less than the characteristic time of $3.16281\ \text{ms}$ for a silver particle with a radius of $3\ \mu\text{m}$ and does not affect the time necessary to calculate the deflection path. In the numerical calculations the time that the particle travelled before reaching the final position was $50.99\ \mu\text{s}$. This time was too small for the dielectrophoretic force to have any significant effects on deflecting particles. For example, the average total deflection distances obtained in the simulation were $0.52039\ \text{nm}$ in the x -direction and $4.49882\ \text{nm}$ in the z -direction. The results were verified by performing a sample calculation of the deterministic deflection model using a dielectrophoretic force, drag force due to helium and gravitational force. The deflection distance was larger in the y -direction, $124.7276\ \text{nm}$, than in the x -direction, $0.452124\ \text{nm}$, and in the z -direction, $0.9881\ \text{nm}$. This was due to the fact that gravitational force ($0.0116496 \times 10^{-9}\ \text{N}$) acted in the y -direction together with the contribution of the drag force due to the helium medium and over shadowed a dielectrophoretic force which were in the x -direction ($-1.19092 \times 10^{-23}\ \text{N}$) and z -direction ($-1.14497 \times 10^{-24}\ \text{N}$).

In conclusion, dielectrophoresis is not an appropriate option that can be used to deflect silver particles in the $1.0\ \text{meter}$ diameter helium hot pipe because it produces nanorange total deflections. It can however be used in microchannels to sort neutral particles according to their sizes because the force depends on the size and electrical properties (dielectric and conductivity constants) of the particle. Therefore, particles of small difference in size would be able to be deflected to different regions and separated. The method may be used to sort particles of the same size based on their difference in dielectric properties. Another method that can be investigated for deflecting charged silver particles in the deterministic deflection model is that of an

electrostatic precipitation (see appendix C). The method determines the deflection of charged particles using parallel plates to produce a uniform electric field. This is because the applied voltage is directly proportional to the deflection distance (see eq. C.10) and an increase in voltage could result in larger deflections.

Bibliography

- [1] Atanasoff J. V., The Dielectric Constant of Helium, *Phys. rev.*, **36**, pg. 1232, (1930).
- [2] Castellanos A., *et al.*, 2003, Electrodynamics and Dielectrophoresis in Microsystems: Scaling Laws *J. Phys. D: Appl. Phys.*, **36**, pp. 2584-2597, (2003).
- [3] Cronje P. M., Verification of Pebble Bed Modular reactor Magnetic Isotope Scrubber - Background and Theory, Verification of PBMR Magnetic Isotope Scrubber- Software, and Verification of PBMR Magnetic Isotope Scrubber- Summary and Results (unpublished internal PBMR report), (2007).
- [4] Crowe C., Elger D., Roberson J., Engineering Fluid Mechanics. 7th Edition., Wiley, New Jersey, (2001).
- [5] Cleveland J. C., ORNL Analysis of AVR Performance and Safety. Proceedings of A Specialists Meeting on Safety and Accident Analysis for Gas-Cooled Reactors, *IAEA-TECDOC-358*, pp. 73-84, (1985).
- [6] Dietrich G., Neumann W., Roehl N., Decommissioning of the Thorium High Temperature Reactor (THTR 300). Technical Committee Meeting on Technologies for Gas Cooled Reactor Decommissioning, Fuel Storage and Waste Disposal, *IAEA-TECDOC-1043*, pp. 9-15, (1997).
- [7] Everett M. R., Kinsey D. V., Römberg E., Carbon Transport Studies for Helium Cooled High Temperature Reactors. D. P. 491, (1966).
- [8] Feeley C. M., Pohl H. A., The Influence of Resistivity and Permittivity on the Motion of Uncharged Solid Particles in Nonuniform Electric Fields (the 'dielectrophoretic effect'), *J. Phys. D: Appl. Phys.*, **14**, pp. 2129-38, (1981).

- [9] Fuller, C. H., Fort Saint Vrain operational experience. Technical Committee on Design Requirements, Operation and Maintenance of Gas-cooled Reactors, **IWGGCR-19**, pp. 5561, (1988).
- [10] Ghosh T. K., and Prelas M. A., Energy Resources and Systems: Fundamentals and Non-Renewable Resources, **1**, *Springer Science + Business Media B.V*, (2009).
- [11] Hinds C. W., Properties, Behaviour, and Measurement of Airborne Particles, Aerosol Technology, Second Edition, John Wiley and Sons, INC, (1999).
- [12] Hook J., Hall H., Solid state physics, 2nd Edition, Wiley, Chichester, (1996).
- [13] Howatson A., An Introduction to Gas Discharge. Pergamon Press, London, (1965).
- [14] Huang Y., Pethig R., Meas. Sci. Tech., **2**, pp. 1142-1146, (1991).
- [15] International Atomic Energy Agency (IAEA), Fuel Performance and Behavior in Gas Cooled Reactors, *IAEA-TECDOC-978*, (1997).
- [16] Integrated Engineering Software, Electro V6.0 2D/RS Field Simulator, Electro Users and Technical Manual, Canada,1985. (<http://www.integratedsoft.com/Products/Electro>.)
- [17] Jackson J. D., Classical Electrodynamics, Second Edition, Wiley and Sons, INC, (1975).
- [18] Jones T., Electromechanics of Particles. Cambridge University Press, New York, (1995).
- [19] Kadak, A. C., A Future for Nuclear Energy: Pebble Bed Reactors. *Int. J. Critical Infrastructures*, **1(4)**, pp. 330-345, (2005).
- [20] Kadaksham A., Sing P. and Aubry N., Dielectrophoresis of Nanoparticles. *Electrophoresis*, **25**, pp. 3625-3632 (2004).
- [21] Kang K., Xuan X., Kang Y. and Li D., Effects of dc-Dielectrophoretic Force on Particle Trajectories in Microchannels, *J. Appl. Phys.*, **99**, (2006).
- [22] Kheswa B. V., Deflection of Ag-atoms in an Inhomogeneous Magnetic Field, Masters Thesis, Department of Physics, University of Stellenbosch, (2011).

- [23] Kingrey K. I., Fuel Summary for Peach Bottom Unit 1 High-Temperature Gas Cooled Reactor Cores 1 and 2. Idaho National Engineering and Environmental Laboratory, *INEEL/EXT-03-00103*, (2003).
- [24] Kugeler K., Stulgies A., Epping C., Aerosol Formation During Water Ingress into the Core of a Pebble Bed High-Temperature Reactor. *Aerosol Science and Technology*, **9**, pp. 177-187, (1988).
- [25] Kruger K. J., Ivens G. P., Safety-related Experiences with the AVR Reactor. Proceedings of A Specialists Meeting on Safety and Accident Analysis for Gas-Cooled Reactors, *IAEA-TECDOC-358*, pp. 61-70, (1985).
- [26] Leu T. S., Chen H. Y., *et al.*, Design and Simulation of Continuous Dielectrophoretic Flow Sorter, *J. Mech.*, **22**, pp. 235-45, (2006).
- [27] Lide D., CRC Handbook of Chemistry and Physics. 77th Edition. CRC Press, New York, (1996).
- [28] Lin J. T. *et al.*, Cell Manipulations with Dielectrophoresis, (Unpublished thesis presented to the University of Waterloo), (2007).
- [29] Martzer D., Pebble Bed Modular Reactor Project Status and the Way Ahead, Second International Topical Meeting on High Temperature Reactor Technology, Beijing China, **no. A04**, pp. 22-24, (2004).
- [30] Mihai L., Separation of Small Metallic Nonferrous Particles in Low Concentration from Mineral Wastes using Dielectrophoresis, **78**, pp. 215-216, (2006).
- [31] Min-Soo K. *et al.*, Experimental and Theoretical Analysis of DEP-based Particle Deflection for the Separation of Protein-bound Particles, *J. Micromech. Microeng.*, **19**, pg. 9, (2009).
- [32] Mills A. F., Heat Transfer, Second Edition, Printice Hall, (1999).
- [33] Moore W., Physical Chemistry, 3rd Edition, Longmans, Green and Co., London, (1957).
- [34] Moormann R., Fission Product Transport and Source Terms in HTRs: Experience From AVR Pebble Bed Reactor. *Science and Technology of Nuclear Installations*. *Doi:10.1155/2008/597491*, (2008).

- [35] Mokhantshang J. K., Masters Thesis, Evaluation of the Efficiency of Magnets in Deflecting Ag-atoms in the Pebble Bed Modular Reactor Magnetic Isotope Scrubber (MIS), Masters Thesis, North West University, (2008).
- [36] Parker K., Electrical Operation of Electrostatic Precipitators, Institute of Electrical Engineers, London, (2003).
- [37] Pereiro M., Baldomir D., Structure of Small Silver Clusters and Static Response to an External Electric Field, *Phys. Rev. A*, **75**, pp. 1-9, (2007).
- [38] Petti et. al., Key Differences in the Fabrication, Irradiation and Temperature Accident Testing of U.S and German Triso-coated Particle Fuel and their Implication on Fuel Performance, 1st International topical Meeting on High Temperature Reactor Technology, *Nuclear Engineering and Design*, **222**, pp. 281-297, (2003).
- [39] Pethig R., Dielectrophoresis: Using Inhomogeneous AC Electrical Fields to Separate and Manipulate Cells, **16**, pp. 331-348, (1996).
- [40] Pohl H. A., Some Effects of Nonuniform Electric Fields on Dielectrics, *J. Appl. Phys.*, **29**, pp. 1182-1188, (1958).
- [41] Pohl H. A., Dielectrophoresis: The Behavior of Neutral Matter in Nonuniform Electric Fields, Cambridge University Press, (1978).
- [42] Ponomarev-Stepnoi. *et al.*, Development of Fast Helium Reactors in Russia, *Atomic energy*, **94 (No.4)**, pp. 262-270, (2003).
- [43] Ramos A., Morgan H., *et al.*, AC Electrokinetics: A Review of Forces in Microelectrode Structures, *J. Phys. D: Appl. Phys.*, **31**, pp. 2338-2353, (1998).
- [44] Roellig K., The THTR-300 Coolant Gas Activity, an Indicator of Fuel Performance. Proceedings of a Specialists Meeting on Behavior of Gas Cooled Reactor Fuel under Accident Conditions, *IWGGCR-25*, pp. 99-108, (1990).

- [45] Scütze A., Jeong J., Babayan S., Park J., Selwyn G. and Kicks R., The Atmospheric-Pressure Plasma Jet: A Review and Comparison to other Plasma Sources. *IEEE Trans. Plasma Sci.*, (1998).
- [46] Sears F., An Introduction to Thermodynamics, the Kinetic Theory of Gasses, and Statistical Mechanics. Second Edition, Addison-Wesley, (1964).
- [47] Slabber J., Pebble Bed Fuel Advantages, Second International Topical Meeting on High Temperature Reactor, Beijing, Applied physical techniques, *Fisika G 530-8-STA*, no. **B15**, pp. 22-24 (2004).
- [48] Stempniewicz M. M., Komen E. M. J., and de With A., Model of Particle Resuspension in Turbulent Flows. *Nuclear Engineering and Design*, **238**, pp. 2943-2959, (2008).
- [49] Steyn H. J., et. al., Particle Deflection and Plate-out Dynamics in a Helium Stream, Masters Thesis, University of Stellenbosch, (2009).
- [50] Takamatsu K., Nakagawa S., Takeda T., Development of Core Dynamics Analysis of Coolant Flow Reduction Tests of HTTR. Proceedings HTR2006: Third International Topical Meeting of High Temperature Reactor Technology, Johannesburg, South Africa, (2006).
- [51] Taylor D., Secker P., Industrial Electrostatics: Fundamentals and Measurements. Wiley, Taunton, (1994).
- [52] U.S. Department of Energy, A Technology Roadmap for Generation IV Nuclear Energy Systems. U.S. DOE Nuclear Energy Research Advisory Committee and the Generation IV International Forum, December 2002, GIF-002-00, (2002).
- [53] van der Merwe J. J., Development and validation of fission product release models and software at PBMR, Paper No: C: 18. 2nd International topical meeting on high temperature technology, Beijing China, September 22, (2004).
- [54] Venneri F., Deep-burn: Destruction of Nuclear Waste and Recycle of Resources using MHR Technology. IAEA, (2005).
- [55] Wang X., Yang J. *et al.*, Cell Separation by Dielectrophoretic Field-Flow-Fractionation, *Anal. Chem.*, **72**, pp. 832-839, (2000).

- [56] Wichner R. P., Fission Product Plateout and Liftoff in the MHTGR Primary System: A Review. Oak Ridge National Laboratory, *NUREG/CR-5647, ORNL/TM-11685, R1, R7, R8*, (1991).
- [57] Zheng Y., Shi L., Dong Y., Thermohydraulic transient studies of the Chinese 200 MWe HTR-PM for loss of forced cooling accidents, *Nuclear Engineering and Design*, **239**, pp. 1212-1219, (2009).
- [58] Zhang Z., Xu Y., Sun Y., et. al., Current status and technical description of Chinese 2×250 MWth HTR-PM demonstration plant, *Nuclear Engineering and Design*, **239**, pp. 1212-1219, (2009).

Appendix A

A.1 Derivations From Basic Principles

Appendix A is used to derive a number of equations using first order analysis or basic principles. These derived equations are used in chapter 2 and 3. The velocity profile between two flat plates determined in this section was needed in eq. (2.59) for the helium velocities. The dielectrophoretic derivation explains and motivates the assumptions made in deriving eq. (2.38). To validate the assumption that particles reach their terminal velocity quickly, the terminal velocity was investigated together with the time it takes to reach it depending on the particle size.

A.1.1 Derivation of Flow Velocity Profile Equation

Since velocities are unchanging with time and unchanging along the tube, the momentum conservation principle reduces to a simple force balance. Accordingly, a force balance is made on an elemental fluid element, which has a length of Δx and is located between radii r and $r + \Delta r$, as shown in figure A.1. The pressure and viscous forces acting on the element are balanced such that their sum equals zero as

$$[2\pi r \Delta r P]_r + \left[2\pi r \Delta x \left(-\mu \frac{dv}{dr} \right) \right]_{x+\Delta x} - \left[2\pi r \Delta x \left(-\mu \frac{dv}{dr} \right) \right]_{r+\Delta r} = 0 \quad (\text{A.1})$$

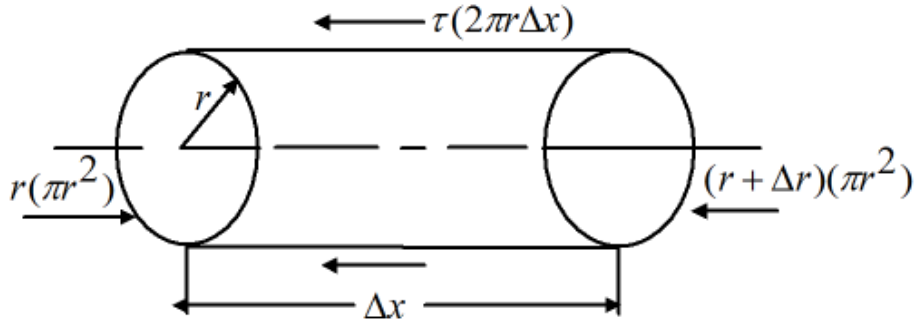


Figure A.1: The force balance on the fluid element to determine the velocity profile using two parallel plates.

Then if we divide equation A.1 by $2\pi\Delta r\Delta x$ and rearrange the final equation, the results can be written as

$$\frac{r\mu \frac{dv}{dr}|_{r+\Delta r} - 2\pi r \Delta r \mu \frac{dv}{dr}|_r}{\Delta r} = \frac{rP|_{x+\Delta x} - rP|_x}{\Delta x} \quad (\text{A.2})$$

By letting $\Delta r, \Delta x \rightarrow 0$ the eq. (A.2) can be written as

$$\frac{d}{dr}(r\mu \frac{dv}{dr}) = r \frac{dP}{dx} \quad (\text{A.3})$$

Eq. (A.3) is the desired differential equation to solve for the velocity profile and since $\frac{dP}{dx}$ is a constant for hydrodynamically fully developed flow, it is a second-order ordinary differential equation for $v(r)$. The two boundary conditions required to solve eq. (A.3) are

$$r = 0 : \quad \frac{dv}{dr} = 0 \quad (\text{A.4})$$

$$r = R : \quad v = 0 \quad (\text{A.5})$$

The first integration of eq. (A.3) and rearranging gives

$$\frac{dv}{dr} = \frac{r}{2\mu} \frac{dP}{dx} + \frac{C_1}{r\mu} \quad (\text{A.6})$$

Then using the first boundary condition (A.4) gives $C_1 = 0$. While, the second integration gives

$$v = \frac{r^2}{4\mu} \frac{dP}{dx} + C_2 \quad (\text{A.7})$$

and the second boundary condition (A.5) gives C_2 as

$$C_2 = -\frac{R^2}{4\mu} \frac{dP}{dx} \quad (\text{A.8})$$

When eq. (A.8) is substituted back into eq. (A.7), it gives the velocity profile as

$$v(r) = \frac{R^2}{4\mu} \left(-\frac{dP}{dx}\right) \left[1 - \left(\frac{r}{R}\right)^2\right] \quad (\text{A.9})$$

The maximum velocity is on the centerline, where $r = 0$, and is given as

$$v_{max} = \frac{R^2}{4\mu} \left(-\frac{dP}{dx}\right) \quad (\text{A.10})$$

The bulk velocity is the area-weighted average velocity and here the bulk velocity is set to the average velocity as

$$v_b = v_{ave} = \frac{1}{2} v_{max} = \frac{R^2}{8\mu} \left(-\frac{dP}{dx}\right) \quad (\text{A.11})$$

The velocity profile $v(r)$ is then conveniently expressed in terms of the average velocity as

$$v(r) = 2v_{ave} \left(1 - \left(\frac{r}{R}\right)^2\right) \quad (\text{A.12})$$

Figure A.2 shows helium Poiseuille flow velocity profile of helium medium between two parallel plates with a height (h) of 10 cm.

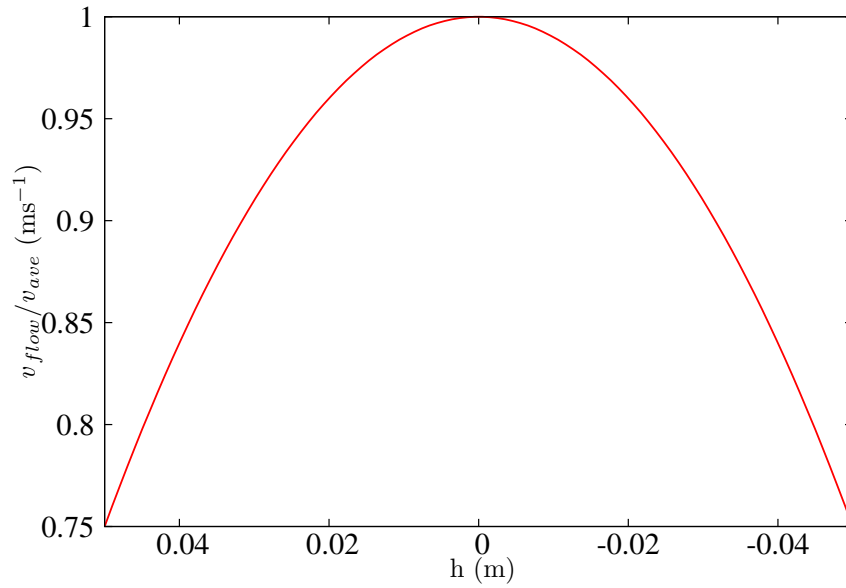


Figure A.2: Helium Poiseuille flow profile normalized by the average velocity (v_{flow}/v_{ave}) from eq. (A.12) between two infinite parallel plates. The height (h) of the parallel plates is 10 cm.

A.1.2 Terminal Velocity

In this section the terminal velocity and time needed for a particle subject to a constant acceleration to reach its terminal velocity are derived. When a particle accelerates it experiences a drag force that increases as the velocity increases. This acceleration occurs until the particle reaches terminal velocity where the drag force is equal to the acceleration force (Cro01). Replacing the applied force in eq. (2.56) with a gravitational force minus the hydrodynamic drag force gives

$$m_p \frac{dv_p}{dt} = F_g - F_{stokesdrag}. \quad (\text{A.13})$$

Assuming that the Reynolds number is less than 0.5 and Stokes' drag force holds. The time the particle takes to reach a drag force of say 95 % of the gravitational force can be calculated from a rearranged version of eq. (A.13) (Ste09), and then integrating as follows

$$\frac{m_p}{6\pi\mu R} \int_0^{\frac{0.96F_g}{6\pi\mu R}} dv_p = \int_0^{t_t} dt, \quad (\text{A.14})$$

where t_t is the time necessary for the particles drag force to reach 95 % of its acceleration force or in other words, the time required to *nearly* reach terminal velocity. This leads to the time to terminal velocity as

$$t_t = 3 \frac{m_p}{6\pi\mu R}. \quad (\text{A.15})$$

Table A.1 shows a few values t_t that have been calculated using eq. (A.15). These values suggests that the smaller the particle the quicker it reaches terminal velocity. The equation can be written in a modified version called the characteristic time (Kan06) in order to determine whether a particle reaches terminal velocity. The characteristic time scale is given as (Ste09)

$$t_{scale} = \frac{m_p}{6\pi\mu R} \quad (\text{A.16})$$

where μ is the dynamic viscosity. The characteristic time calculated using eq. (A.16) should be an order of magnitude smaller than the time of the numerical calculations to conclude that a particle reaches terminal velocity. If that condition is certified then the incremental equations for the particle's velocity in chapter 2 can be used, otherwise, eq. (2.56) must be used (Kan06).

Table A.1: Values of t_t for different particle radii using eq. (A.15). The density, ρ , of the particle is 10500 kg/m⁻³, and the viscosity μ (of temperature 300 K and 1 atmosphere pressure) is 20.1×10⁻⁶ kgms⁻¹.

R m	t_t s
10×10^{-9}	3.48259×10^{-8}
100×10^{-9}	3.48259×10^{-6}
200×10^{-9}	1.39303×10^{-5}
3000×10^{-9}	3.16281×10^{-3}
4000×10^{-9}	5.57213×10^{-3}

A.1.3 Dielectrophoresis derivation

This section provides a detailed derivation of the effective dipole moment \mathbf{p} acting on a spherical particle (Jon95). This derivation provides a better understanding of the physics behind dielectrophoresis. Figure A.3 shows a spherical particle (e.g. silver) with radius r and permittivity ϵ_{Ag} placed in helium gas with

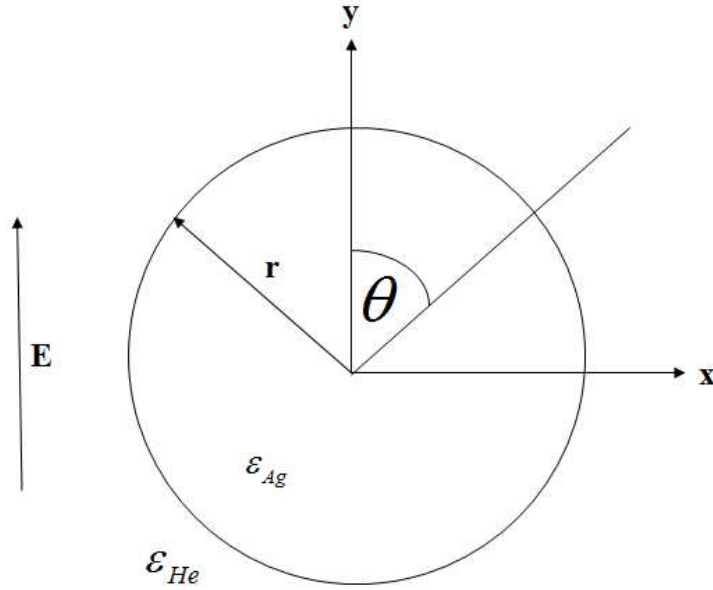


Figure A.3: Spherical silver particle of radius R and permittivity ϵ_{Ag} immersed in helium and subjected to a uniform electric field (Jon95).

permittivity ϵ_{He} , and subjected to a nonuniform electric field \mathbf{E} . The charge distribution within the particle will vary. If the assumption is made that the charge of nearby particles does not influence the charge distribution, the electric potential outside ϕ_1 and inside ϕ_2 the particle can be written as (Jon95)

$$\phi_1(r, \theta) = -Ercos\theta + \frac{Acos\theta}{r^2}, \quad r > R \quad (\text{A.17})$$

$$\phi_2(r, \theta) = -Brcos\theta \quad r < R \quad (\text{A.18})$$

where θ and r are the polar coordinates. The first term of eq. (A.17) is the imposed uniform electrostatic field and the second term is the particles' induced dipole charge. The electric potential is the same at the surface, which leads to the boundary value of $\phi_1(r = R, \theta) = \phi_2(r = R, \theta)$. When this boundary condition is applied to eq. (A.17), it leads to

$$-Ercos\theta + \frac{Acos\theta}{r^2} = -Brcos\theta \quad (\text{A.19})$$

The flux density is defined as the density of the flux lines passing through a specific point (Tay94), it must be continuous across a boundary which leads to continuity boundary conditions (Jon95)

$$\varepsilon_{He} \frac{\partial \phi_1}{\partial r} = \varepsilon_{Ag} \frac{-\partial \phi_2}{\partial r} \quad (\text{A.20})$$

Inserting eq. (A.20) into the differentiated form of eq. (A.18) gives

$$\left(-E \cos \theta + \frac{2A \cos \theta}{r^3} \right) \varepsilon_{He} = \varepsilon_{Ag} (-B \cos \theta) \quad (\text{A.21})$$

In eq. (A.21) a division on both sides by $\cos \theta$ gives an expression written in terms of constant B as

$$B = \left(E - \frac{2A}{r^3} \right) \frac{\varepsilon_{He}}{\varepsilon_{Ag}} \quad (\text{A.22})$$

A substitution of eq. (A.22) in eq. (A.19) and dividing both sides by $\cos \theta$ gives

$$-Er + \frac{A}{r^2} = - \left(E - \frac{2A}{r^3} \right) \frac{\varepsilon_{He}}{\varepsilon_{Ag}} r \quad (\text{A.23})$$

Further manipulation of eq. (A.23) results in an equation written in terms of constant A as

$$A = \frac{\varepsilon_{Ag} - \varepsilon_{He}}{\varepsilon_{Ag} + 2\varepsilon_{He}} r^3 E \quad (\text{A.24})$$

The effective dipole moment (Jon95) can be expressed in terms of A as

$$m_{eff} = 4\pi \varepsilon_{He} A. \quad (\text{A.25})$$

Inserting eq. (A.24) into the effective dipole moment eq. (A.17) and (A.25) gives

$$m_{eff} = 4\pi \varepsilon_{He} \frac{\varepsilon_{Ag} - \varepsilon_{He}}{\varepsilon_{Ag} + 2\varepsilon_{He}} r^3 E. \quad (\text{A.26})$$

Eq. (A.25) can be written in terms of the Mossotti factor K_{CM} as

$$m_{eff} = 4\pi r^3 \varepsilon_{He} K_{CM} E \quad (\text{A.27})$$

where K_{CM} is given as

$$K_{CM} = \frac{\varepsilon_{Ag} - \varepsilon_{He}}{\varepsilon_{Ag} + 2\varepsilon_{He}}. \quad (\text{A.28})$$

Appendix B

B.1 Numerical Programs and Flow Charts

Appendix B is used to describe the numerical algorithms used in both the stochastic and deterministic simulations. These algorithms are written in the Python and C programming languages and a summary of the key steps are given in each case.

B.2 Numerical Algorithm for Stochastic Model

The main program is written in C programming. It uses a number of subroutines to perform the calculations. In the program the subroutines involved in the simulations are the velocity distribution sampler, silver particle movement due to electric field and the collision generator. In the main program all parameters are initialized accordingly and the algorithm is as follows:

- Initialize helium temperature T and pressure P .
- Initialize molecular weight of silver M_{Ag} and helium M_{He} .
- Initialize diameter of silver d_{Ag} and helium d_{He} atoms.
- Calculate the probable velocity v_p and average velocity v_{ave} of the particles
- Calculate the time τ between collisions using the mean freetime eq. (2.14).

- Perform simulations for a specified elapsed time and allow collision at the end of the mean free time.
- Produce the probable speed, average velocity, deflection distance and mean free time.
- end program

The stochastic model simulations can be summarized using a flow chart (see figure B.1) to show the link between different algorithms and the procedure followed. The description of the deterministic model's numerical algorithms is given in section B.3.

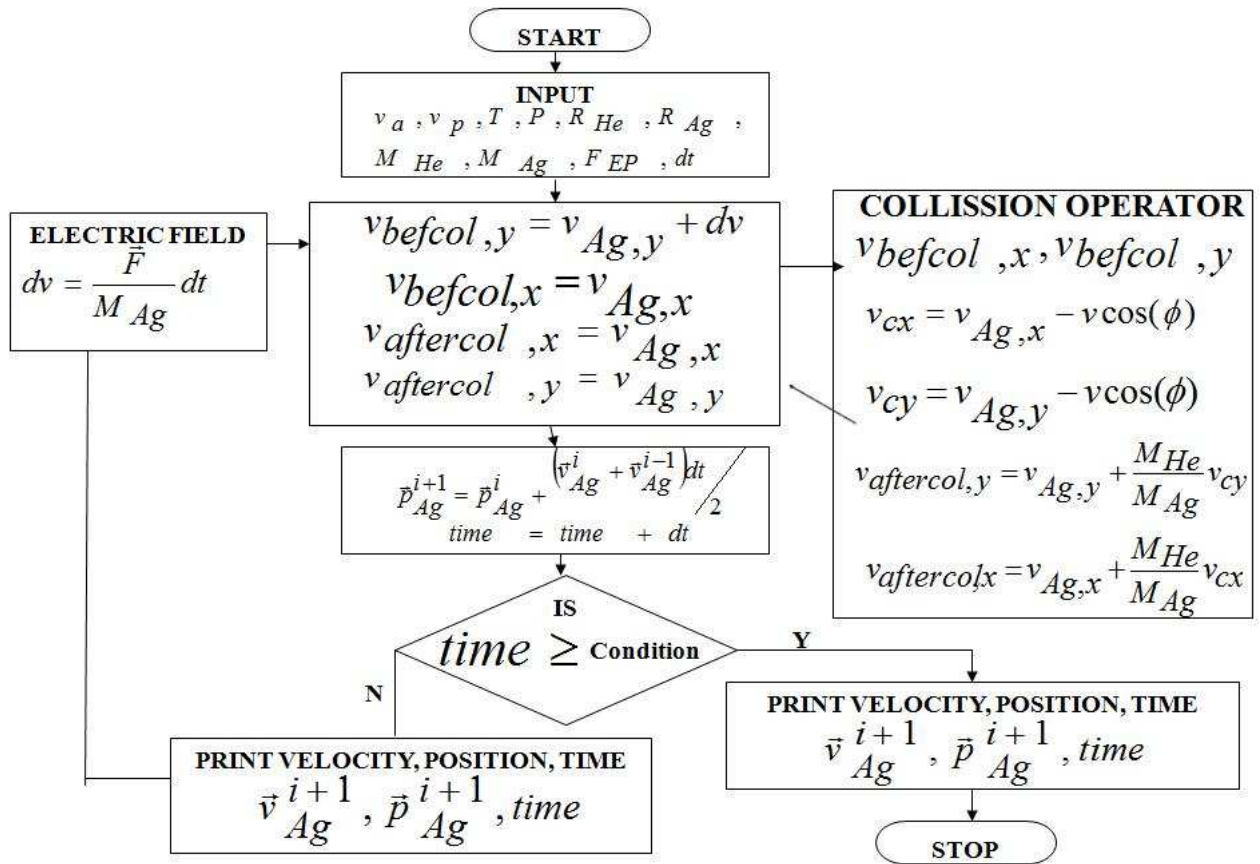


Figure B.1: A schematic representation of the algorithm used in the stochastic numerical simulations.

B.3 Numerical Algorithm for Deterministic Model

This section describes an algorithm for the deterministic deflection simulations. The program reads nonuniform electric field data produced independently using *Electro V6.2 software*. The motion of the particle is tracked in the helium medium using eq. (2.56). A brief summary of the key steps in the main program are given:

1. Define all the variables needed in the program.
2. Initialize all necessary values required.
3. Calculate all constants required for the simulation.
4. Obtain initial position of the particle in the system.
5. Perform the following iterations as long as the particle has not touched the wall:
 - Calculate the dielectrophoretic forces in the direction of the field used to deflect the particle.
 - Calculate the gravitational force and the drag force in the direction of flow.
 - Calculate the position of the particle due to dielectrophoresis, gravity and drag force.
 - Keep track of the time it takes to complete the numerical calculations.
 - Write data to file for plotting and analysis.
6. Stop the program.
7. End the program.

The deterministic model numerical algorithm like the stochastic part can be summarized using a flow chart to show how the program flows. Figure B.2 shows the flow chart for the deterministic numerical algorithm.

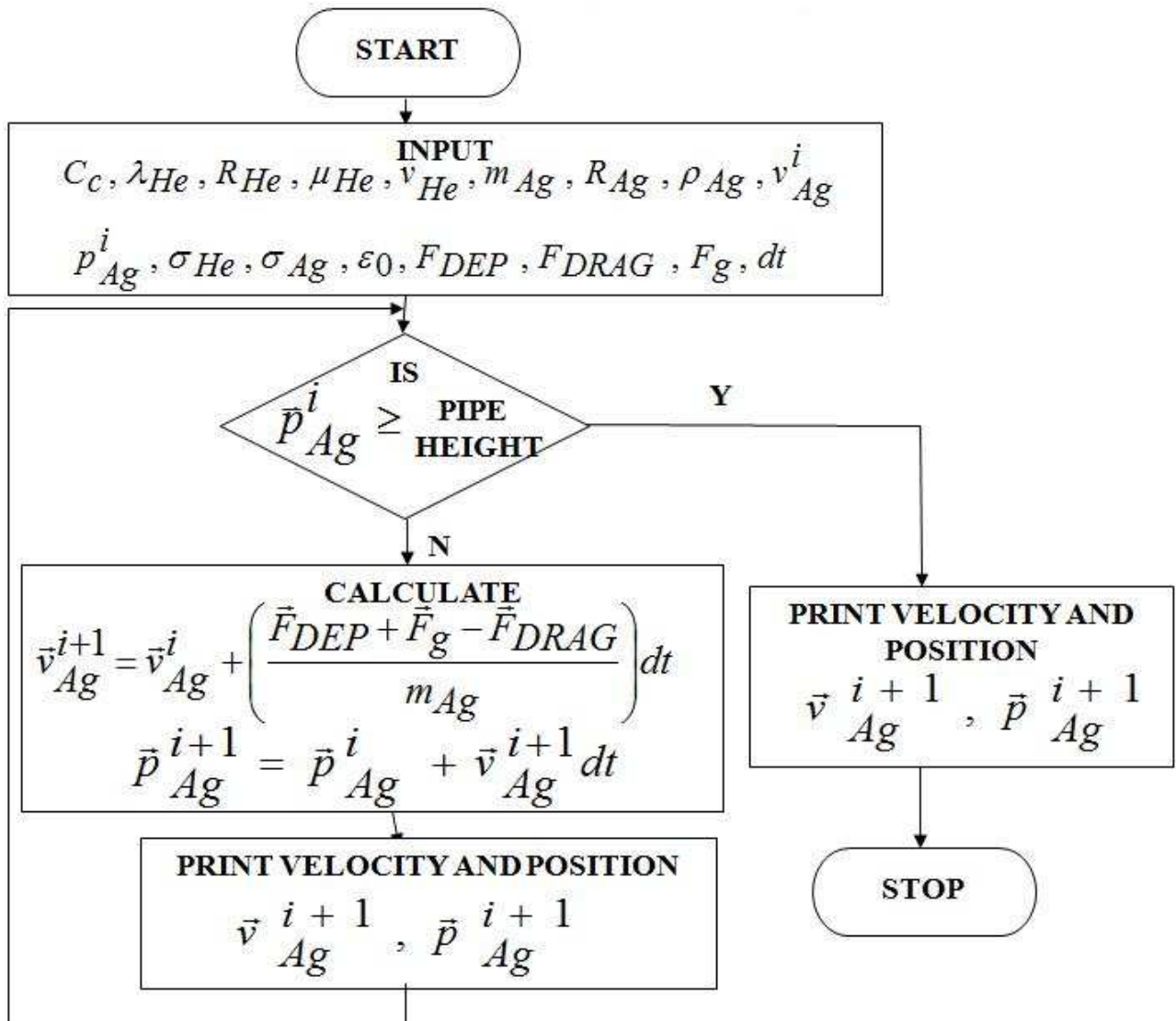


Figure B.2: A schematic representation of the algorithm used in the deterministic numerical calculations.

Appendix C

C.1 Electrostatic Precipitation

In this section a deflection model is developed using two parallel plates (10 cm) to produce a uniform electric field. The model investigates movement of the aerosol particle as it is deflected by a uniform electric field in a helium medium that is flowing laminarly through the two parallel plates. The uniform electric field is created by applying a voltage (1 kV and 2 kV) between the plates so that the field is vertically perpendicular to the helium flow streamline. The motion of the particle in the x -direction (see figure C.1) is without any applied forces and the governing equation is given as

$$m \frac{d^2x}{dt^2} = 0. \quad (\text{C.1})$$

Eq. (C.1) is solved by integrating twice and setting the velocity v_x as the flow velocity of the helium medium.

The first integration of eq. (C.1) gives

$$\frac{dx}{dt} = v_x = v_{flow} \quad (\text{C.2})$$

The final result for the position of a particle in the x -direction is

$$x(t) = x_0 + (v_{flow})t. \quad (\text{C.3})$$

where x_0 is the initial position of the particle, and v_{flow} is the helium velocity and t is the time as the particle travels in the medium. The motion of the particle in the y -direction is determined from the balance between the aerodynamic drag and electrostatic forces. The aerodynamic drag force (\mathbf{F}_D) can be represented in terms of the electrical mobility of the particle and will be balanced by the electrostatic force (\mathbf{F}_{ES}). The governing equation is written explicitly and assuming that the particle settles, then acceleration is negligible as

$$m \frac{d^2 y}{dt^2} = F_D - F_E \quad (C.4)$$

$$= \left(\frac{qe}{Z_p} \right) \left(\frac{dy}{dt} \right) - (qeE) \quad (C.5)$$

$$= - \left(\frac{qe}{Z_p} \right) \left(\frac{dy}{dt} \right) - \left(\frac{qeV}{d} \right) \approx 0. \quad (C.6)$$

The last part of eq. (C.6) defines the motion of the particle in the y -direction and is a differential expression of the first order

$$- \left(\frac{qe}{Z_p} \right) \left(\frac{dy}{dt} \right) - \left(\frac{qeV}{d} \right) = 0, \quad (C.7)$$

Eq. (C.7) is rearranged and written as

$$\frac{dy}{dt} = - \frac{Z_p V}{d}, \quad (C.8)$$

After rearranging eq. (C.8) then the expression can be integrated using separation of variables as

$$\int_{y_0}^y dy = - \frac{Z_p V}{d} \int_0^t dt, \quad (C.9)$$

The end result is the position of the particle in the y -direction as

$$y(t) = y_0 - \frac{Z_p V}{d} t. \quad (C.10)$$

where y_0 is the initial position of the particle in the direction of the electric field, Z_p is the electrical mobility (discussed in section C.1.1), V is the voltage applied on the plates, d is the diameter of the particle, and t is the time as the particle travels in the helium medium. Since the vertical velocity is inversely proportional

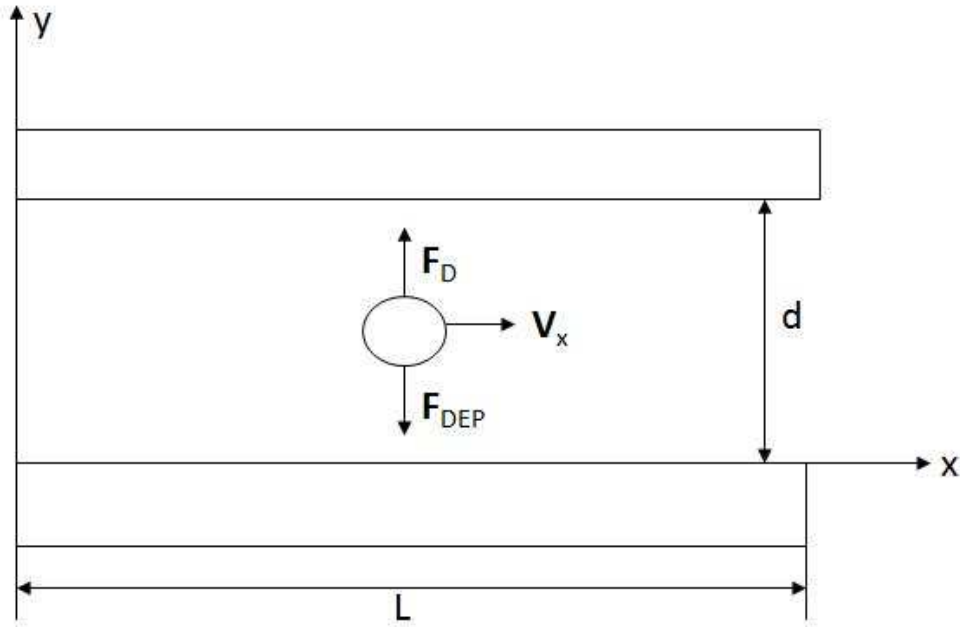


Figure C.1: Two dimensional system of electrostatic precipitation.

to the separation distance, the smallest allowable value of d was chosen to provide fast particle collection. A number of concepts that have been used in this section are discussed properly in the next section, and these are the electrical mobility and the slip correction factor.

C.1.1 Electrical Mobility

Electrical mobility is the charged particles ability (such as electrons or protons, ions or clusters) to move through media when acted upon by an electric field that is acting on the particle in a particular direction (Hin99). In order to determine the electrical mobility (Z), it is noted that when a charged particle is placed in an electric field, it experiences a force F_{ES} given as

$$\mathbf{F}_{ES} = ne\mathbf{E} \quad (\text{C.11})$$

where n is number of charge units, e is the universal electron charge and \mathbf{E} is the electric field. For particle motion in the Stokes' region the terminal electrostatic velocity V_{TE} is obtained by equating the electrostatic

force eq. (C.11) and the Stokes drag eq. (2.44) such that

$$V_d = \frac{(ne\mathbf{E}C_c)}{(3\pi\eta d)}. \quad (\text{C.12})$$

Then the ability of a particle to move in an electric field in terms of electrical mobility, Z , the velocity of a particle with a given charge ne and in an electric field of unit strength can be written according to its mobility as follows

$$Z = \frac{V_d}{E} = \frac{(neC_c)}{(3\pi\eta d)}. \quad (\text{C.13})$$

Electrical mobility is proportional to the net charge of the particle. This was the basis for Robert Millikan's demonstration that electrical charges occur in discrete units ($1e$, $2e$, $3e$, and so on), whose magnitude is the charge of the electron (Hin99). For spherical particles much larger than the mean free path of the molecules of the medium, Z is inversely proportional to the diameter of the particles and when the spherical particles are much smaller than the mean free path, Z is inversely proportional to the square of the particle diameter.

C.1.2 Slip Correction Factor

The Cunningham slip correction factor (also called Cunningham's correction factor) accounts for molecular slip which occurs when particle size is of the same magnitude as the distance between gas molecules. The particle no longer moves as a continuum in the gas, but as a particle among discrete gas molecules thereby reducing the drag force. Correction factor is used to account for noncontinuum effects when calculating the drag on small particles. The derivation of Stokes Law, which is used to calculate the drag force on small particles, assumes that the relative velocity of the gas right at the surface of the sphere is zero. This assumption is not correct for small particles whose size approaches the mean free path of the gas because such particles settle faster than predicted by Stokes law due to slip at the surface of the particle. The error becomes large for particles less than $1 \mu\text{m}$ in diameter (Hin99). The correction factor that takes into accounts this effect is given as

$$F_D = \frac{3\pi\eta V d}{C_c} \quad (\text{C.14})$$

and C_c is given as follows

$$C_c = 1 + \frac{2.52\lambda}{d} \quad (\text{C.15})$$

where λ and d are the mean free path of the gas and the diameter of the particle, respectively. Eq. (C.15) extends the region of application of Stokes law to particles of 0.1 diameter. However, the empirical equation (Hin99) of the slip correction factor that provides an extension of the Stokes law to particle range of below 0.01 μm is written as

$$C_c = 1 + \frac{\lambda}{d} \left[2.514 + 0.800 \times \exp\left(-0.55\frac{\lambda}{d}\right) \right]. \quad (\text{C.16})$$

C.1.3 Electrophoresis Numerical Method

An electrophoresis technique is used in the deterministic model to study the effects of an external uniform electric field on a charged particle moving in a helium medium. Herein, a single particle is selected and its trajectory determined as it is deflected by the electric field. The total deflection distance of the particle is recorded with the total time it takes to cover the distance in the direction of flow or motion (x -direction) for plotting. The simulations are performed within a region of the applied electric field. The particle experiences a drag force in the helium medium. The setup is a two dimensional parallel electrodes used to produce a uniform electric field placed on the surface of the helium medium. In the system eq. (C.10) and (C.3) are used to numerically calculate the solution for motion of the particle under the influence of a uniform electric field.

C.1.4 Assumptions

The calculations are based upon a two dimensional model. The particle is initially located at a specific height between the two parallel plates, when entering the region of an applied uniform electric field representing the longest particle path. Some of the assumptions made in the numerical calculations are:

- The flow profile is a parabolic helium velocity profile.
- Initially, in the x -direction the particle moves along the streamline.

- Particles quickly reach terminal velocity in the Stokes region.
- Gas velocity dependent on height following the helium velocity profile.
- Electric field is everywhere vertical, perpendicular to streamlines.
- Gravitational settling and diffusion losses are negligible.

C.1.5 Results

Using eq. (C.3) and (C.10) the trajectory of a 3 μm charged particle are obtained. The results obtained numerically from electrostatic Precipitation are presented in table C.1. The modelled values obtained for different uniform electric field strengths show that the time taken to deflect a single clustered particle depends directly on the applied voltage and total charge of the particle. The total time taken to deflect a particle and the total deflection distance achievable are shorter when the voltage is increased (see table C.1). This implies that as the voltage is increase (e.g. from 1kV to 2kV) the particle are deflected faster and cover a larger distance in the direction of the electric field but force the particle to cover a shorter distance in the direction of flow or motion in the process. Figure C.2(a) shows the relationship between the total deflection distance and the total time taken to deflect the particle at an applied voltage of 1 kV and figure C.2(b) shows the same results at an applied voltage of 2 kV. The helium medium acts as a drag force and slows down the particle. However, significant deflections can be achieved by further increasing the voltage.

Table C.1: Electrostatic precipitation numerical results for a 3 μm charged particle. The helium bulk velocity is 0.012 ms^{-1} . The total deflection distance in the direction of the electric field is 10 cm.

Voltage = 1 kV		Voltage = 2 kV	
Distance meters	Time seconds	Distance meters	Time seconds
0.000476581	0.0529535	0.000238291	0.0264767
0.000238291	0.0264767	0.000119145	0.0132384
0.00015886	0.0176512	7.94302×10^{-05}	0.00882558
0.000119145	0.0132384	5.95727×10^{-05}	0.00661919

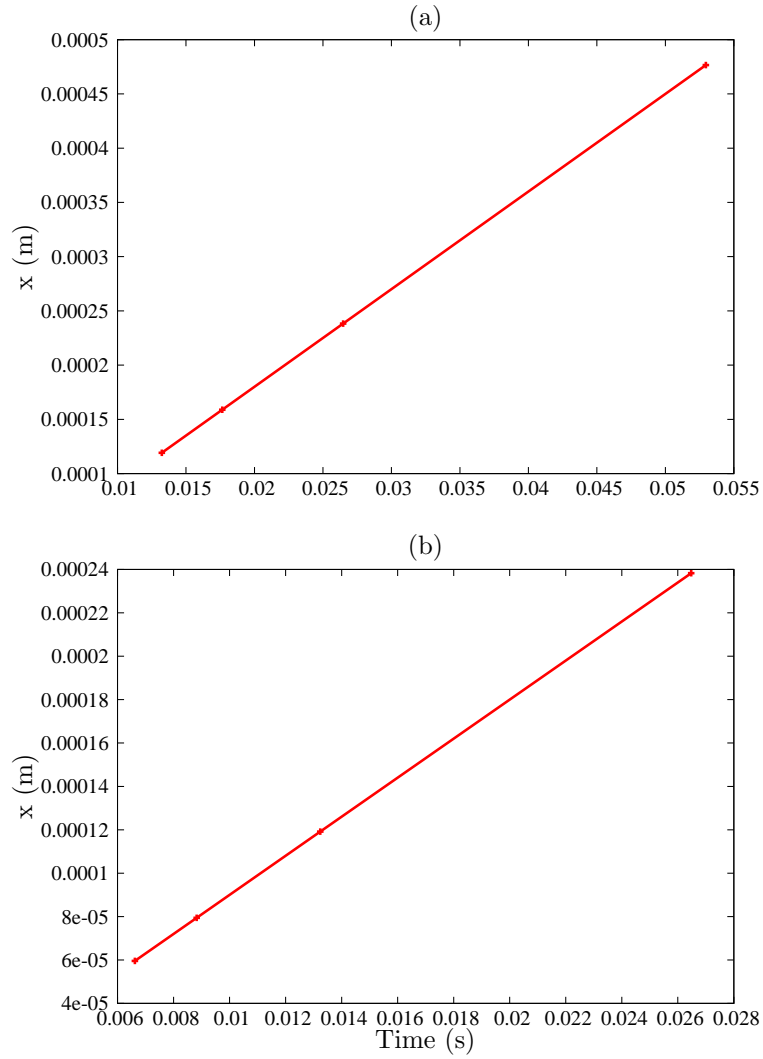


Figure C.2: The relationship between the total distance travelled in the x -direction (x is the direction of flow or motion) for a $3 \mu\text{m}$ charged particle and the total time taken to travel the distance, with an applied voltage of (a) 1 kV and (b) 2 kV. The helium bulk velocity is 0.012 ms^{-1} and the height between the parallel plates is 10 cm.